HELLENIC MEDITERRANEAN UNIVERSITY

DEPARTMENT OF ELECTRONIC ENGINEERING

MASTER THESIS

Tracking, analysis, and interference with FEM solution

subdomains of laser assisted machining simulations.

Baroutsos Andreas

Rethymno, 2020

A. Baroutsos
Tracking, analysis, and interference in FEM solution subdomains in simulations of laser assisted machining.

ippl

A. Baroutsos
Tracking, analysis, and interference in FEM solution subdomains in simulations of laser assisted machining.

ippl

HELLENIC MEDITERRANEAN UNIVERSITY

DEPARTMENT OF ELECTRONIC ENGINEERING

MASTER THESIS

Tracking, analysis, and interference with FEM solution

subdomains of laser assisted machining simulations.

Baroutsos Andreas

Advisory Committee
Prof. Vasilios Dimitriou
Prof. Michael Tatarakis
Prof. Efthimios Bakarezos

Examination Committee
Prof. Vasilios Dimitriou
Prof. Michael Tatarakis
Prof. Emmanouil Benis

A. Baroutsos
Tracking, analysis, and interference in FEM solution subdomains in simulations of laser assisted machining.

ippl

Acknowledgements

I would like to express my gratitude to my supervisor Prof. Vasilis Dimitriou for his support and essential guidance during my master thesis, as well for the opportunities he provided me during my studies, and he continues to provide. He believed in me even when I had fewer time to study due to my daily work and family, compared to a full-time student. I would like to thank Dr Evaggelos Kaselouris because without his assistance this thesis would never be completed. He spent many hours to provide me with the proper FEM knowledge and guidance. I must thank the team of IPPL for their teamwork and support. I would like also to thank Commander Antonis Koundourakis GRC Navy, because without his assistance and his understanding my MSc would not be completed.

Special thanks must be given to my wife Cristina Alexandri and my daughter Olga Baroutsou for their love, for their support, for their patience and for the countless hours they missed me.

A. Baroutsos
Tracking, analysis, and interference in FEM solution subdomains in simulations of laser assisted machining.

ippL

Abstract

The present thesis is focused on the simulations of laser Assisted Machining by the Finite Elements Method. FEM allow us to track and analyze maximum interest sub-regions of the laser Assisted Machining simulation experiment, and the ability of interference with the global simulated problem. Two representative models are used to demonstrate the LAM simulation by FEM. Linux bash scripts are developed to track and analyze the user defined maximum interest sub-regions of LAM, based on the temperature thresholds as criterion, during the runtime of the solution. Finally, Linux bash scripts are developed for LAM on AISI H-13 steel to modify the initial conditions and parameter values of the originally set FEM problem, like temperature and laser heat flux intensity. These values are used in the subdomains of interest, to modify the initial simulation by restarting the problem, at simulation time-steps where the real problem parameters change. These scripts will be further used in the future for the interconnection of MD and MHD simulations with FEM.

A. Baroutsos
Tracking, analysis, and interference in FEM solution subdomains in simulations of laser assisted machining.

ippι

Περίληψη

Η παρούσα εργασία επικεντρώνεται στις προσομοιώσεις Κατεργασιών Υποβοηθούμενων από Λέιζερ (LAM) με τη Μέθοδο των Πεπερασμένων Στοιχείων (FEM). Η FEM μας επιτρέπει να παρακολουθούμε και να αναλύουμε τις υπό-περιοχές μέγιστου ενδιαφέροντος του LAM πειράματος προσομοίωσης και παρέχει την ικανότητα παρέμβασης στο καθολικό πρόβλημα που μοντελοποιείται. Χρησιμοποιούνται δύο αντιπροσωπευτικά μοντέλα για την παρουσίαση της προσομοίωσης LAM με FEM. Bash Linux scripts αναπτύσσονται για να παρακολουθούν και να αναλύουν τις καθορισμένες από το χρήστη υπό-περιοχές μέγιστου ενδιαφέροντος της LAM, με βάση τα όρια θερμοκρασίας ως κριτήριο, κατά το χρόνο εκτέλεσης της προσομοίωσης. Τα bash Linux scripts εκτελούνται προσομοίωση LAM χάλυβα AISI H-13 για την τροποποίηση των αρχικών συνθηκών και των τιμών παραμέτρων του αρχικά καθορισμένου προβλήματος FEM, όπως η θερμοκρασία και η ένταση ροής θερμότητας λέιζερ. Αυτές οι τιμές χρησιμοποιούνται στους υπό-τομείς ενδιαφέροντος, για την τροποποίηση της αρχικής προσομοίωσης με επανεκκίνηση του προβλήματος, σε χρονικά βήματα προσομοίωσης όπου αλλάζουν οι παράμετροι του πραγματικού προβλήματος. Αυτά τα σενάρια θα χρησιμοποιηθούν περαιτέρω στο μέλλον για τη διασύνδεση προσομοιώσεων MD και MHD με FEM.

A. Baroutsos
Tracking, analysis, and interference in FEM solution subdomains in simulations of laser assisted machining.

ippl

Table of Contents

A. Baroutsos
Tracking, analysis, and interference in FEM solution subdomains in simulations of laser assisted machining.

ippl

A. Baroutsos
Tracking, analysis, and interference in FEM solution subdomains in simulations of laser assisted machining.

ippl

List of figures

A. Baroutsos
Tracking, analysis, and interference in FEM solution subdomains in simulations of laser assisted machining.

ippl

List of tables

A. Baroutsos
Tracking, analysis, and interference in FEM solution subdomains in simulations of laser assisted machining.

ippl

List of Symbols

chip	Part of the material that is removed during cutting procedures
LAM	Laser Assisted Machining
FEM	Finite Elements Method
FE	Finite Element
laser	Light Amplification by Stimulated Emission of Radiation
MASER	Microwave Amplification by Stimulated Emission of Radiation
CW	Continues Wave
EM	Electromagnetic
CPA	Chirp Pulse Amplification
COTS	Commercial off-the-shelf
HPC	High-Performance Computers
LAMM	laser assisted micro-machining
JC	Johnson-Cook empirical material model
AISI	American Iron and Steel Institute
PCBN	Polycrystalline Cubic Boron Nitride
ASCII	American Standard Code for Information Interchange
HAZ	Heat Affected Zone
MD	Molecular Dynamics
MHD	Magnetohydrodynamics
AOI	Area Of Interest
OS	Operating System
HPC	High-Performance Computing
CAE	Computer Aided Engineering
SMP	Symmetric Multiprocessing
MPP	Massively Parallel Processors
MPI	Message Passing Interface
V-M	Von Mises

A. Baroutsos
Tracking, analysis, and interference in FEM solution subdomains in simulations of laser assisted machining.

ippu

xii

A. Baroutsos
Tracking, analysis, and interference in FEM solution subdomains in simulations of laser assisted machining.

ippu

Chapter 1

1 Introduction

1.1 Machining

The production of almost any modern item is based on machining. Nowadays, the modern technologies have boosted the machining processes and new parts can be created fast and efficiently. Furthermore, difficult to cut materials, like titanium alloys and ceramics, may be machined as common materials for the produce of new parts and items which in the past we could not even imagine using them in our everyday life.

1.1.1 Machining processes

During machining, a product, or a part of a product, is manufactured by material removal. Most products are initially manufactured in their first form by methods that do not involve cutting. After a product is made in its primary shape, machining and other mechanical processes, that mostly remove mass from the product, are applied to finalize the products design. The manufacturing processes can be divided to six categories: i. Casting, ii. Forming and shaping, iii. Machining, iv. Joining, v. Finishing and vi. Microfabrication and nanofabrication, with the category iii. of Machining, to be outstanding as the most important and complex.

There are various cutting processes that can be classified as machining processes, as shown in figure 1.1. This thesis is focused on the cutting process of turning. All the cutting processes may be split in two categories, namely the orthogonal and the oblique cutting, which are described in sections 1.1.2 and 1.1.3, respectively.

A. Baroutsos
Tracking, analysis, and interference in FEM solution subdomains in simulations of laser assisted machining.

ippl
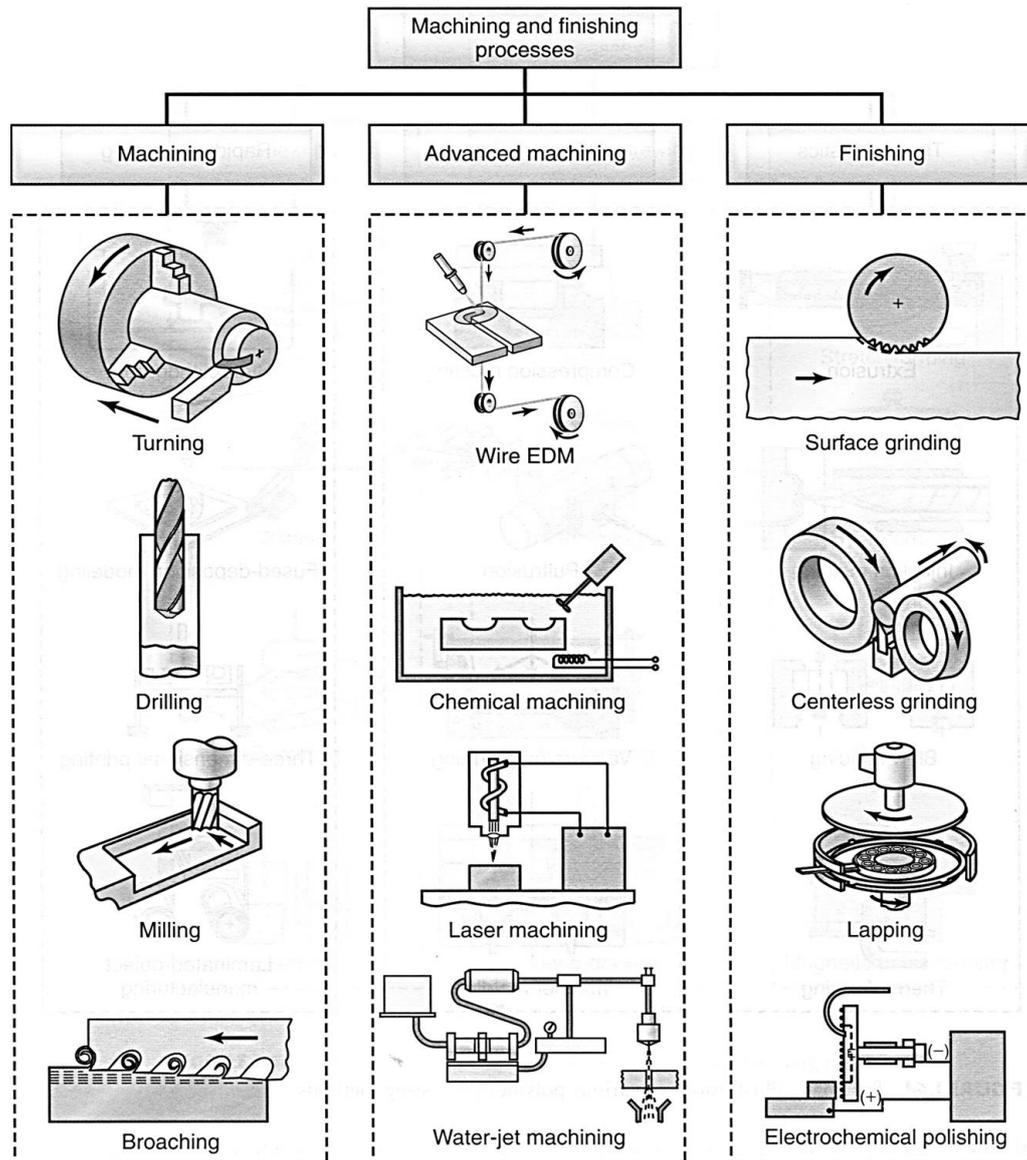
Figure1.1 Categories of the machining processes [1]

1.1.2 Orthogonal cutting

In orthogonal cutting, it is assumed that the cutting process takes place in two dimensions and thus the simulation models are two dimensional and thus, the cutting and the thrust forces are perpendicular, while in oblique cutting the tool is considered to be three dimensional. Therefore, the part of the material that is removed during cutting, the chip, is helical in oblique, in contradiction to the chip produced in orthogonal cutting, where chips' shape is restricted on the 2D plane. Figure 1.2 presents the orthogonal (left) and the oblique (right) cutting. This Thesis is focused on the orthogonal cutting and therefore the feed rate and the depth of cut are equal.

A. Baroutsos
Tracking, analysis, and interference in FEM solution subdomains in simulations of laser assisted machining.

ippl
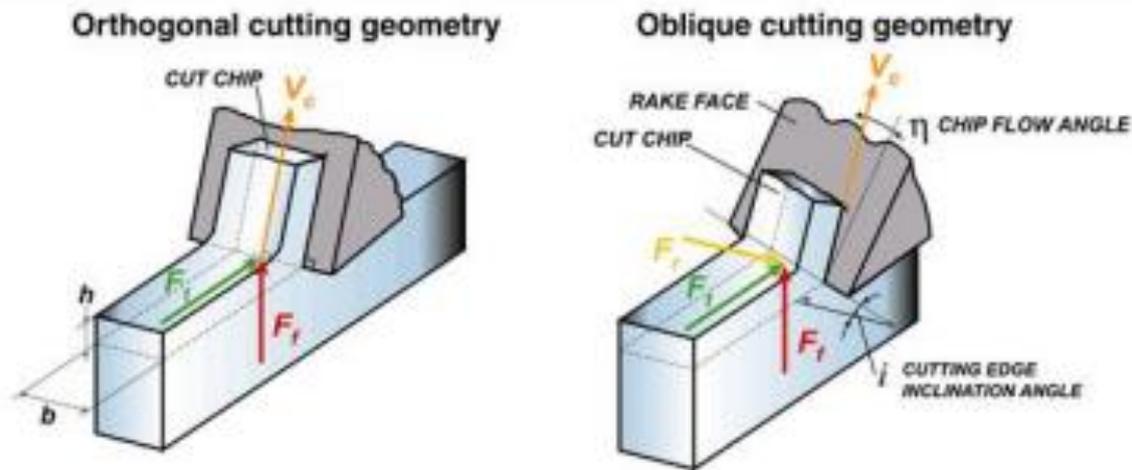
Figure 1.2 Orthogonal and Oblique cutting[1]

The are many parameters and factors that affect machining. These parameters and factors can be divided into two categories, the independent and the dependent variables of the cutting process [1].

Independent	Dependent
Tool material and coatings	Type of chip produced
Tool shape, surface finish and sharpness	Force and energy dissipated during cutting
Workpiece material and condition	Temperature rise in the workpiece, the tool and the chip
Cutting speed, feed and depth of cut	Tool wear and failure
Cutting fluids	Surface finish and surface integrity of the workpiece
Characteristics of the machine tool	
Work holding and fixturing	

Table 1.1 Machining independent and dependent variables of the cutting process

This Thesis is focused on dependent parameter of the Temperature that rise in the workpiece and the chip. This parameter is strictly related to laser Assisted Machining (LAM), and furthermore affects the cutting tool life and the physical and mechanical characteristics of

---

[1] Webpage https://vivadifferences.com/difference-between-orthogonal-cutting-and-oblique-cutting/ last access 22 June 2020

A. Baroutsos
Tracking, analysis, and interference in FEM solution subdomains in simulations of laser assisted machining.

iPPL

the workpiece (see figure 1.3 for instance). When temperature rises, the strength and hardness of the cutting tool decreases, thus resulting to wear resistance decrease. Similar phenomena occur for the workpiece, increasing the machinability and the ability to be cut easier, faster and more efficiently. All the above take place in thermal conditions that do not exceed a certain threshold, which is different for every material. Above this threshold the workpiece and/or the cutting tool lose their integrity and might be destroyed.
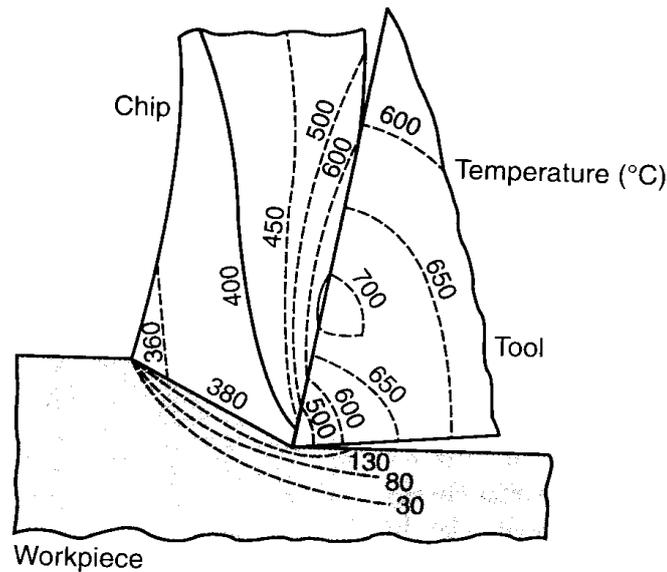
Figure 1.3 Temperature distribution in the cutting zone during conventional machining [1]

1.2   Lasers

The LAM process is based on the assistance of a laser, the Light Amplification by Stimulated Emission of Radiation, a device that after its invention, has been applied to every aspect of our modern life, since it is used from stellar observation, to telecommunications and cosmetics.

1.2.1 Laser history

The theoretical background for laser was the work of Albert Einstein for the process of stimulated emission. The invention of laser was founded on the invention of Microwave Amplification by Stimulated Emission of Radiation (MASER) [2]. After that, the same technique was applied to infrared and optical light resulting to laser [3]. In 1960 the first ruby laser was constructed by Theodore Maiman. He won the race against Townes and Schawlow,

A. Baroutsos
Tracking, analysis, and interference in FEM solution subdomains in simulations of laser assisted machining.

ippl

and he excited atoms in artificial ruby medium crystal resulting to a short burst of concentrated light. Later that year the first CW (Continuous Wave) gas laser was invented by Javan, Benett and Herriott. After this event the evolution of that technology was abrupt. Nowadays they can be found everywhere. They can be simple gadgets in our pockets to illuminate our presentations or modern scalpel of the surgeons or powerful energy transferring devices that may initiate ultra-high energy conditions like the beginning of our cosmos.

1.2.2 Laser physics

The main idea is based on the Alberts Einstein stimulated emission, that means, where an excited atom or molecule deexcites and at least a photon is emitted. The photon characteristics (wavelength etc.) are based on the quantum mechanics and the thermodynamic attributes of that atom or molecule. This procedure is divided into three steps. Firstly, an atom is excited by a photon of at least the exact amount of energy that needs to be excited. Secondly, another photon interacts with the stimulated atom and finally two photons of $E_2 - E_1 = \Delta E = hf$ are generated. This chain reaction amplifies the total energy of the light that is produced, leading to the creation of the laser beam.

The energy in eV is : $\Delta E_{(eV)} \simeq \frac{1.2}{\lambda_{(\mu m)}}$ $where\ \lambda f \simeq 3x10^8 \frac{m}{s}$ and λ is the wavelength of the emitted light. Nowadays laser systems emit peak power from 2 PW in University of Osaka to less than 1 mW. They are also been categorized based on the duration of their pulse, from femtosecond $10^{-15}s$ to CW.

Important aspects of the laser light are the spatial coherence and the temporal coherence. Spatial coherence means that the light is very tightly focused. The temporal coherence means that the laser light is monochromatic, having very narrow EM spectrum, or wide EM spectrum existence in techniques that produce femtosecond pulses. These techniques are called ultrashort pulse techniques, and one of them is Chirp Pulse Amplification or CPA.

Simplest laser design consists of the pump source that is the gain medium and the amplifier that is the part that drives that EM wave repeatedly through the gain medium to amplify its energy.

In LAM CW laser is used since stable flow of energy and power is demanded.

A. Baroutsos
Tracking, analysis, and interference in FEM solution subdomains in simulations of laser assisted machining.

ippl

1.3 LAM

Many methods are developed to improve efficiency of the machining processes. Some of them are: LAM, chemical machining, electrical discharge machining, plasma assisted machining, thermally assisted machining, and abrasive machining. LAM is a hybrid method that combines conventional machining and laser light, to enhance cutting tool material removal. The increase of temperature in order to make machining easier is an idea that emerged at the 1940 machining workshops and laboratories [1]. The workpiece was heated with various ways to increase machinability. LAM constitutes the evolution of these efforts. laser provides its unique characteristics in benefit of the cutting process. It can be tightly focus on the spot of interest and heat only the wanted part of the workpiece. The main feature of the LAM process is the reduction of the cutting forces via increasing the temperature of the workpiece to reduce the strength of the material. This strength reduction causes the reduction of the material hardness and the tool's wear. Thus, the machinability of the workpiece is increased, the tool life is extended, and surface finish is improved, while high material removal rate is achieved [6,8,9]. figure 1.4 shows schematically the LAM process and the cutting parameters of laser spot diameter d_s, temperature t_s and workpiece feedrate f.

To further explore the LAM method and to reduce the performance cost of a large majority of experiments, numerical simulation is a valuable tool for this complex hybrid method of machining.
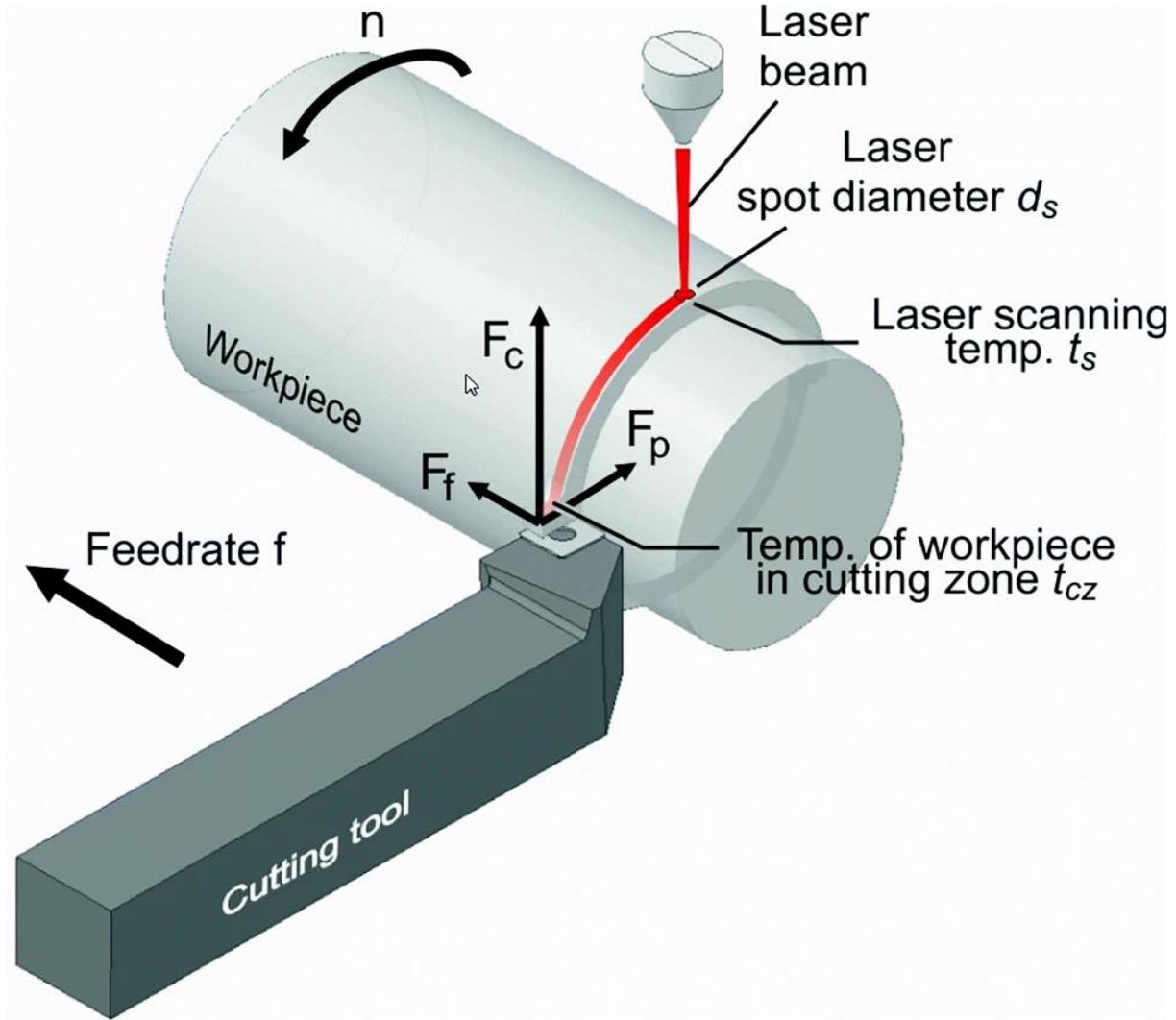
A. Baroutsos
Tracking, analysis, and interference in FEM solution subdomains in simulations of laser assisted machining.

ippl

Figure 1.4 Schematic setup and process parameters of laser assisted turning [2]

A. Baroutsos
Tracking, analysis, and interference in FEM solution subdomains in simulations of laser assisted machining.

ippl

Chapter 2

2 The Finite Element Method

Finite Element Method or FEM can numerically simulate engineering, physics, multiphysics and coupled field problems. Characteristic areas of interest include structural analysis, heat transfer, fluid flow, mass transport and electromagnetism. FEM solves partial differential equations in two or three space variables. With the assistance of modern computational power, this method constitutes the main numerical tool to solve fast and with high accuracy problems that 50 years ago their solution was impossible.

2.1 Historical review of FEM

The first who developed the principles of FEM was the German mathematician Ritz in 1909 [3]. Next step was made by the Russian mathematician Galerkin, who published an article about methods for solving boundary value problems with differential equations. This was the source of the Galerkin method, where a continuous problem is converted to a discrete one and finally linear algebra is used for the solution of differential problems [4]. In 1943 the German mathematician Richard Courant proposed a method for solving numerically partial differential equations [5]. He applied that method at solving torsion problems using triangular elements and using the principle of the minimum potential energy. Two years ago Galerkin, in 1941, the Russian-Canadian engineer Alexander Hrennikoff, presented the lattice analogy for his D.Sc thesis [6], where beam or surface bend problems were modeled by beams. Then a big problem came up, the lack of capable machines to make all these calculations, when the size of the fem grid became higher than a few elements. This forced engineers, mathematicians and physics scientists to postpone the further development of the FEM and its implementation to various fields of research and engineering.

The next step in FEM was made during 1950's. The aeronautics companies, especially their defense department and the birth of electronic computers which allowed fast calculations, provided the resources to restart the FEM development [7]. M. J. Turner while working in Boing was the man that restarted the use of FEM. He optimized the Direct Stiffness Method with the work of B. M. Irons, R. J. Melosh and of the civil engineer E. L. Wilson the developer of an open-source FEM software for structural analysis. All this work was monitored by

A. Baroutsos
Tracking, analysis, and interference in FEM solution subdomains in simulations of laser assisted machining.

ippl

academics of various scientific fields who were transferring the developed knowledge in all sciences.

The Greek civil engineer J.H. Argyris, was one of the first researchers that used a computer to solve structural problems and published [8] many articles (1954) for the use of matrices and FEM, since he was working in the airspace industry as an advisor of Boing. The Americans M. J. Turner, R. W. Clough, H. C. Martin, and L. C. Topp, wrote an article [9] that is considered the beginning of FEM in the present form, while in 1960 the American civil engineer R. W. Clough, baptized the method as FEM and the name remains till now. At the same year J.H. Argyris published his book [10] that established the principles of the FEM. Finally, the Polish-British mathematician and civil engineer O.C. Zienkiewicz published the first detailed book on the FEM [11]. All the above academics are the main people behind the transfer of the FEM principles and knowledge from airspace industry to most of the existing scientific fields and research areas.

2.1.1 FEM evolution

From early 1960's till now every major leap in computer science contributed in FEM. At 1951 GM and IBM built DAC-1 to assist design of cars. In 1965 NASA developed NASTRAN (NASA Structural Analysis) software as a structural solver tool. From then till now computers ability to perform fast calculations and FEM are evolving in parallel. Higher discretization can be achieved, and the precision of the solutions increases. The ability to study and focus into spatial sub-domains, where in the real-life experiment is extremely difficult and expensive to set-up a capable measurement system, made FEM a must in all fields of sciences. FEM can study the condition of a model stressed to its limits, without the need to destroy a real one and without costs of money and resources. Airspace, car manufacturing and construction industries save a huge amount of time and money, by minimizing the number of prototypes needed to evaluate the final product.

A. Baroutsos
Tracking, analysis, and interference in FEM solution subdomains in simulations of laser assisted machining.

ιΡΡL

2.2 What is FEM

The basic target of FEM is to simulate a real construction or phenomena by using elements that are interconnected to a finite number of nodes. Hence a real construction or area can be represented. A construction is made from just one entity. FEM artificially divides that one entity in finite pieces and interconnects them in a series of elements. These elements usually are triangles, or four side shaped in a 2D model and the analogous of them in 3D model, for example tetrahedra or hexahedra. Therefore, there is a finite number of equations that must be solved.
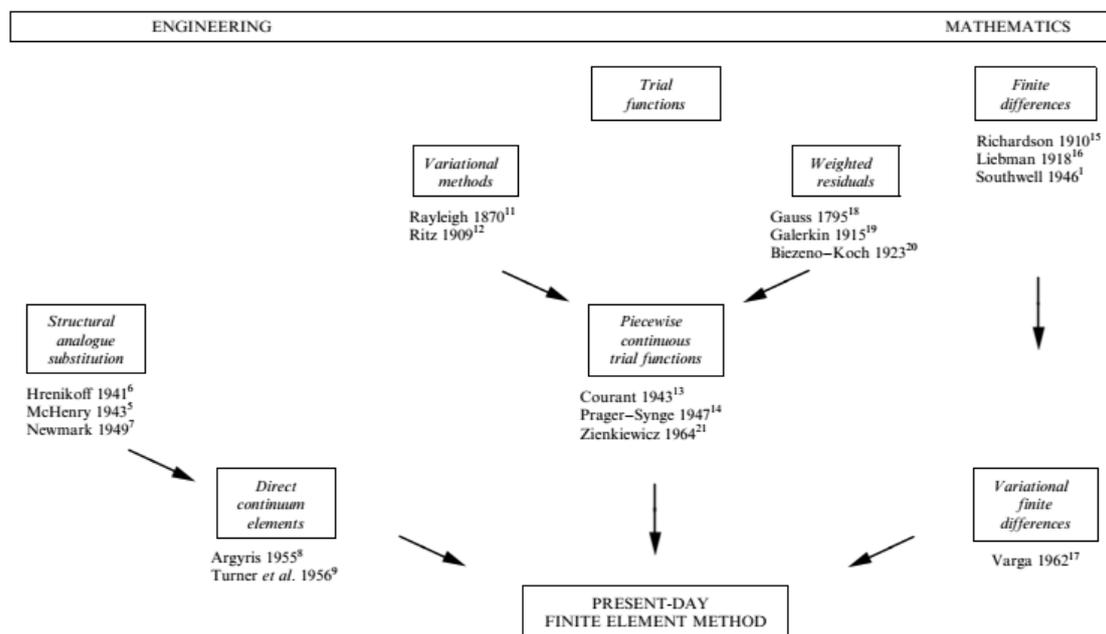
Figure 2.1 The birth and evolution of FEM it reaches its final form [12]

Every FE is also defined by specific material mechanical and physical properties. These properties can be element's thickness, density, Young modulus, Poisson ratio, thermal and electromagnetic properties. For each node corresponds a number of degrees of freedom. These can be the displacements and rotations in three directions, temperature etc.

For structural analysis, matrix analysis that is usually used, is approached by two basic methods, the method of displacements or stiffness and the method of force or flexibility. The displacements method transforms the characteristic differential equations of the structure components, for static analysis, of each FE in the local form $F_{loc} = K_{loc} * U_{loc}$. K_{loc} is defined as the stiffness matrix, F_{loc} is the nodal force matrix applied on the structural component and U_{loc} is defined as the nodal displacement matrix. During structural analysis,

A. Baroutsos
Tracking, analysis, and interference in FEM solution subdomains in simulations of laser assisted machining.

ippl

which consists of many structural components, this equation changes to $F_{glob} = K_{glob} *$ U_{glob}, with the dimensions of K_{glob} matrix to be $kn \times kn$, where n is the total number of nodes and k is the number of degrees of freedom of each node.

Solution can be reached generally by following a few basic steps. First, we assign the type of elements, the material properties and create the geometry of the model in the pre-processor. Next, we assign the boundary and loading conditions and finally, we solve the system with the usage of the global matrix, by assembling the final equations set. Finally, in the post-processor, we gather all the needed output quantities [12].

2.3 FEM modeling of LAM

To study the LAM process two FEM models are used. The first concerns the study of the influence of laser parameters on LAM [13] and the second concerns laser assisted micro-machining (LAMM) [14]. The models are briefly analyzed since we focus on FEM and the model development.

As mentioned in Chapter 1, LAM is a hybrid method combining conventional machining with the usage of laser as a heat source. The numerical modeling is performed using the commercial FEM software LS-DYNA [15]. LS-DYNA is using explicit and implicit numerical solvers to simulate high energy and mass loss problems, like cutting processes, airbag inflations and car crashes. A three-dimensional coupled thermal-structural transient analysis is performed. The workpiece is defined as deformable solid body, the cutting tool as a rigid solid body and the laser beam is modeled as a gaussian moving heat source. The finite element hourglass behavior is implemented in LS-DYNA, with the usage of a control algorithm. It adds viscosity to the hexahedral elements that use reduced integration. Based on the Langragian approach element deletion is allowed (element erosion) when the cutting tool interacts with workpiece. Simultaneously, when elements are eroded, the contact surface is continuously updated. This approach gives more realistic results to the formation and the chip shape, from the incipient stage to a steady form. The distribution and the values of the temperature distribution, plastic strains, Von Mises stresses and cutting forces are analyzed. The moving laser heat source is applied to the model by the following equation:

$$\rho c_p \left(\frac{\partial T}{\partial t} + V_x \frac{\partial T}{\partial x} \right) = \frac{\partial}{\partial x}\left(k \frac{\partial T}{\partial x} \right) + \frac{\partial}{\partial y}\left(k \frac{\partial T}{\partial y} \right) + \frac{\partial}{\partial z}\left(k \frac{\partial T}{\partial z} \right) + \dot{Q}$$

A. Baroutsos
Tracking, analysis, and interference in FEM solution subdomains in simulations of laser assisted machining.

ippl

where ρ, c_p, Vx, k, and $\dot{Q}$ are the density, specific heat, laser scanning speed on the X axis, thermal conductivity, and the rate of volumetric heat generation, respectively. The equation of the momentum is given by the following equation:

$$\rho \frac{\partial^2 U_i}{\partial^2 t} = \mu \frac{\partial^2 U_i}{\partial^2 k} + (\lambda + \mu) \frac{\partial}{\partial i}\left(\frac{\partial U_k}{\partial k}\right) - (3\lambda + 2\mu)\alpha_T \frac{\partial T}{\partial i}$$

where U is the displacement, λ and μ the lame coefficients and α_T the thermal expansion coefficient. The gaussian distribution of the laser beam intensity which provides the absorbed laser heat flux $q(x, z)$ is given by the equation:

$$q(x,z) = \frac{2\eta P_{inc}}{\pi r_b^2} e^{-\left(\frac{2((x-tV_x)^2+z^2)}{r_b^2}\right)}$$

where P_{inc} is the incident laser power, η is the average absorptivity of the workpiece material, t is the time and r_b is the laser beam radius. At the top surface of the workpiece, that is irradiated by laser beam, heat flux is taken into consideration. The equation that considers also convection and the radiation is:

$$-k\frac{\partial T}{\partial y} = q(x,z) - h(T - T_0) - \sigma\varepsilon(T^4 - T_0^4)$$

where h is the convective heat transfer coefficient, T_0 is the ambient temperature, σ is the Stefan–Boltzmann constant (5.67 10^8W/m^{2}K^4) and ε is emissivity.

Apart from the physics model, the material model that is used is the empirical Johnson-Cook (JC) flow stress model [16]. JC gives flow stress using the following equation, taking into consideration the plastic strain, the strain rate and the temperature:

$$\sigma_y = (A + B\varepsilon^n)(1 + Cln\frac{\dot{\varepsilon}}{\dot{\varepsilon}_0})(1 - \frac{T - T_r}{T_m - T_r})^m$$

where ε is the equivalent plastic strain, $\dot{\varepsilon}/\dot{\varepsilon}_0$ is the dimensionless plastic strain rate, $\dot{\varepsilon}_0=1s^{-1}$ is a reference strain rate used to normalize the strain rate, A is the yield stress, B is the hardening constant, C is the strain rate sensitivity, n is the hardening exponent, m is the thermal softening exponent, T_m is the melting temperature of the workpiece and T_r the room temperature. JC is an empirical model, so the material constants A, B, C, n, m is subject of actual experiment results. The J-C material model includes also a fracture model [17] that considers the nucleation, growth and coalescence of voids in a ductile material at high strain rates. It defines the equivalent plastic strain at the onset of damage by the equation:

A. Baroutsos
Tracking, analysis, and interference in FEM solution subdomains in simulations of laser assisted machining.

ippl

$$\varepsilon_f = \left(\left[D_1 + D_2 exp D_3 \frac{p}{\sigma_{VM}} \right] \left[1 + D_4 ln \frac{\dot{\varepsilon}}{\dot{\varepsilon}_0} \right] \left[1 + D_5 \frac{T - T_r}{T_m - T_r} \right] \right), \ D = \sum \frac{\Delta \varepsilon}{\varepsilon_f}$$

where D_1, D_2, D_3, D_4 and D_5 are the failure parameters and σ_{VM} the Von Mises stress. Material fracture occurs when the damage parameter D reaches the value of 1.

These are the common parameters of both models. The next two paragraphs will describe the specific details of the two FEM models for a LAM and LAMM (Laser Assisted Micro-Machining) cases.

2.3.1 LAM of AISI H-13 steel

The workpiece is modelled by 115000 hexahedron solid finite elements, its dimensions are $3.0 \times 0.5 \times 0.5$ mm and the cutting tool is modeled by 35000 hexahedron solid finite elements. The workpiece material is AISI H-13 steel and the cutting tool material is polycrystalline cubic boron nitride (PCBN). The geometry and mesh of the model are depicted in figure 2.2. The translations and rotations of the nodes of the bottom surface of the workpiece are constrained. The Z axis translations on the front and back sides and the X axis translations on the left and right sides are also constrained. The cutting tool dimensions are $20 \times 20 \times 24$ μm, the rake angle is $-5°$, the clearance angle is $5°$, the fillet 0.02 mm radius and is modeled as a rigid body using hexahedral solid finite elements. The rigid body is inserted to a vertical distance from the top surface of the workpiece, denoted as feed, according to the depth-of-cut and its motion is imposed on the X axis. The rest of the material properties, material JC model parameters and failure parameters are shown below:

Property	Workpiece	Tool	Material Model Parameters	Values	Failure Parameters	Values
Density [kg/m^3]	7800	3399	A [MPa]	674.8	D1 [-]	-0.8
Elastic modulus [GPa]	211	652	B [MPa]	239.2	D2 [-]	2.1
Poisson's ratio [-]	0.28	0.128	n [-]	0.28	D3 [-]	-0.5
Specific heat [J/kg K]	560	960	C [-]	0.027	D4 [-]	0.0002
Thermal conductivity [W/m K]	37	100	m [-]	1.3	D5 [-]	2.7
Thermal expansion [10^{-6}C]	10.4					
Melting point [K]	1700					

Table 2.1 Material and JC model parameters values [13]

The laser parameter values are set to a mean absorptivity $\eta=0.5$ and mean emissivity $\varepsilon=0.4$ [18]. The ambient temperature is set to 20 ℃ and the heat transfer coefficient is h=5 W/m^{2}K, for the convectional heat transfer to the surrounding air. The tool is placed 1 mm away

A. Baroutsos
Tracking, analysis, and interference in FEM solution subdomains in simulations of laser assisted machining.

ippl

from the workpiece. The cutting and the laser scanning have the same speed of 150 m/min and the feed rate is 0.15 mm/rev. Coulomb static and dynamic friction coefficients for the tool-workpiece interaction are set to 0.3 [19].
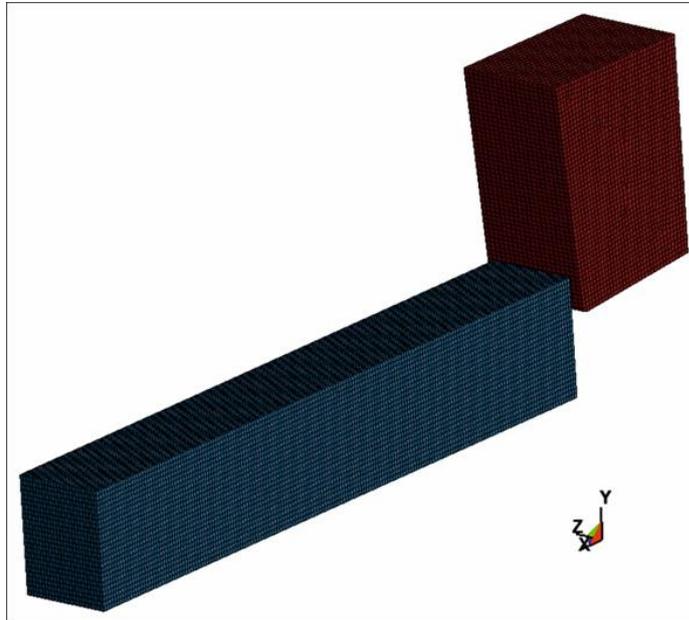

Figure 2.2 Example of orthogonal cutting FEM model, initial stage before cutting [29]

2.3.2 LAMM of AISI H13, AISI 1045 and Ti6AL4V

In LAMM, with the assistance of laser radiation as heat source, we focus to enhance micro-cutting material removal and cutting tool life [14]. We study the generation of HAZ on a metal workpiece, when it is scanned with laser beam, for two scan speeds of 2 and 100 mm/min, resulting in a total simulation time of 240 and 4.8 sec respectively, using three kinds of metal workpieces, AISI H13, AISI 1045 and Ti6AL4V. The workpiece is modelled by approximately 8 million hexahedron solid finite elements. Its dimensions are $8 \times 1 \times 1 \, mm$ with element dimensions $10 \times 10 \times 10 \, \mu m$. The model is half-symmetric to the Z-axis and the motion of the tool is imposed along the X-axis. Material is simulated using the JC model that considers the effect of plastic strain, strain rate and temperature and also includes the effect of fracture by defining the equivalent plastic strain at the onset of damage [19]. The workpiece material properties were set according to literature data, for all three different kind of metals, for JC model including failure parameters, while thermal conductivity, specific heat, thermal expansion and emissivity are considered temperature dependent.

The average absorptivity η of each workpiece material was determined by the comparison of the computed temperature values against the experimentally measured at a

A. Baroutsos
Tracking, analysis, and interference in FEM solution subdomains in simulations of laser assisted machining.

ippl

reference specific workpiece point with common power and speed. The length of laser scanning is 6 mm, its wavelength is 532 nm, and spot diameter is 20 μm. Other parameters are:

a. AISI H13 with P=1 and 2.4 W, Vx=100 mm/min

b. AISI 1045 with P=2.4 W, Vx=2 and 100 mm/min

c. Ti6Al4V with P=1 and 2.4 W, Vx=2 mm/min.

Initially, ambient temperature of 21 ^{o}C is assumed, while constant temperature of 25 ^{o}C is assumed for all sides, except from the symmetry surface.

2.4 Simulation results of the LAM FEM models

The solution of a FEM numerical simulation provides a file or a set of files of solution data. Data in those files are organized in an array or database form, which is either open, like HDF5 or need an advanced 3D visualization package for post-processing from commercial software, such as d3plot files from LS-DYNA. In this thesis, the advanced pre- and post-processor, LS-PREPOST, is used that is delivered free with LS-DYNA. Using LS-PREPOST, the results of the selected physical quantities are exported, for varying timesteps. It is possible to obtain in a single file or in a set of files, the results for every timestep of the solution, in ASCII format. In figure 2.3 typical results of temperature, Von Mises stress and plastic strain are demonstrated for the LAM of AISI H13 steel.
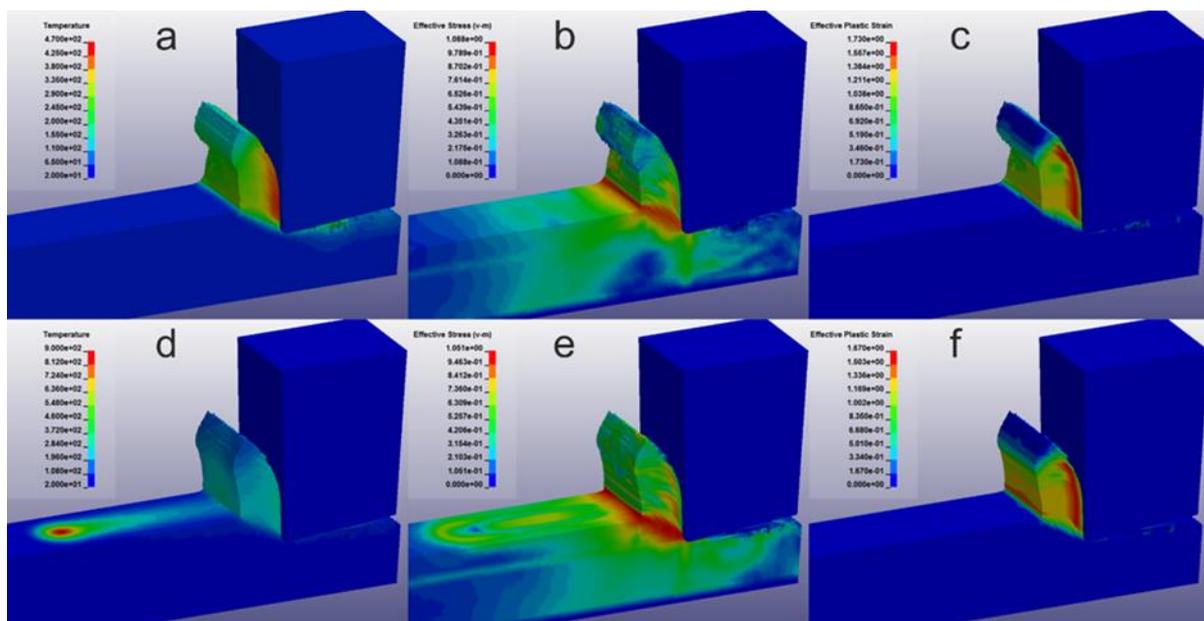

Figure 2.3 Temperature, Von Mises stress and Plastic strain distributions, 0.4 ms after the cutting tool initiation for: (a-c) Conventional (d-f) LAM for laser beam diameter 250 μm and laser power 120 W

A. Baroutsos
Tracking, analysis, and interference in FEM solution subdomains in simulations of laser assisted machining.

ippl

2.4.1 Simulation results of LAM AISI H-13 steel

Two parametric analysis were carried out. In the first case we study the influence of the laser heat flux and in the second the influence of the laser beam diameter. In the first case there was maximum reduction of 14.3% in the thrust force and 6.2% in the cutting force [13]. Results are demonstrated in figure 2.4.
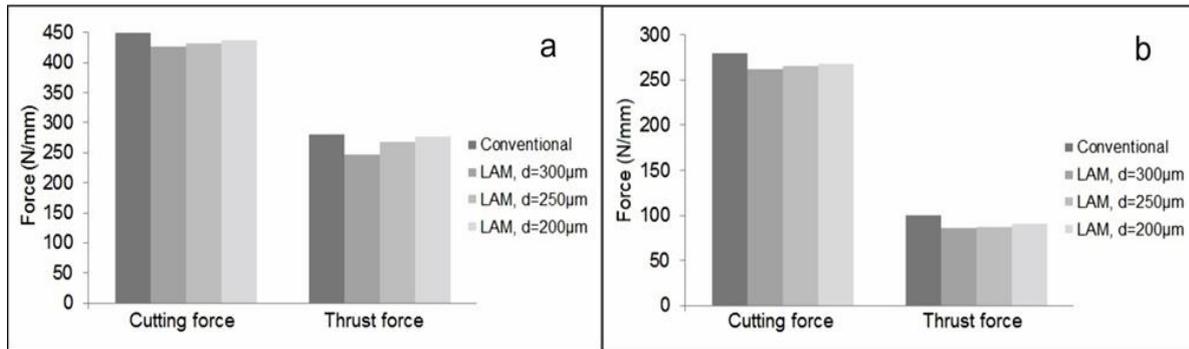

Figure 2.4 Cutting and Thrust force results with constant aser flux of 2 kW/mm^2 compared to conventional cutting for feed rates of a) 0.25 mm/rev and b) 0.15 mm/rev [13]

For the second case there was a maximum reduction 5.4% for the cutting force and 15% for the thrust force. Results are demonstrated in figure 2.5.
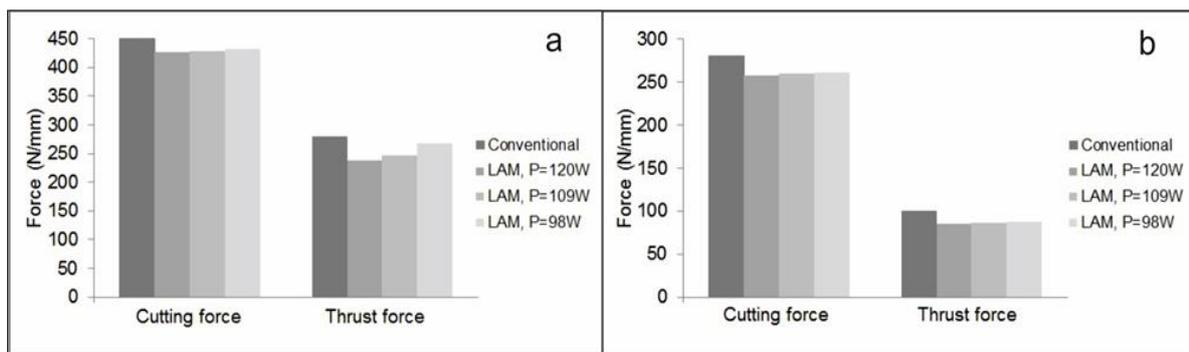

Figure 2.5 Cutting and Thrust force results with constant laser beam radius compared to conventional cutting for feed rates of a) 0.25 mm/rev and b) 0.15 mm/rev [13]

A. Baroutsos
Tracking, analysis, and interference in FEM solution subdomains in simulations of laser assisted machining.

ippl

2.4.2 Simulation results of LAMM

The main research aim is, by validating actual experiment results, to study and determine the optimal laser power, spot diameter and scanning speed values, for each of the three metal workpieces of AISI H13, AISI 1045 and Ti6AL4V that are simulated. Representative results are shown in Figs. 2.6 and 2.7.
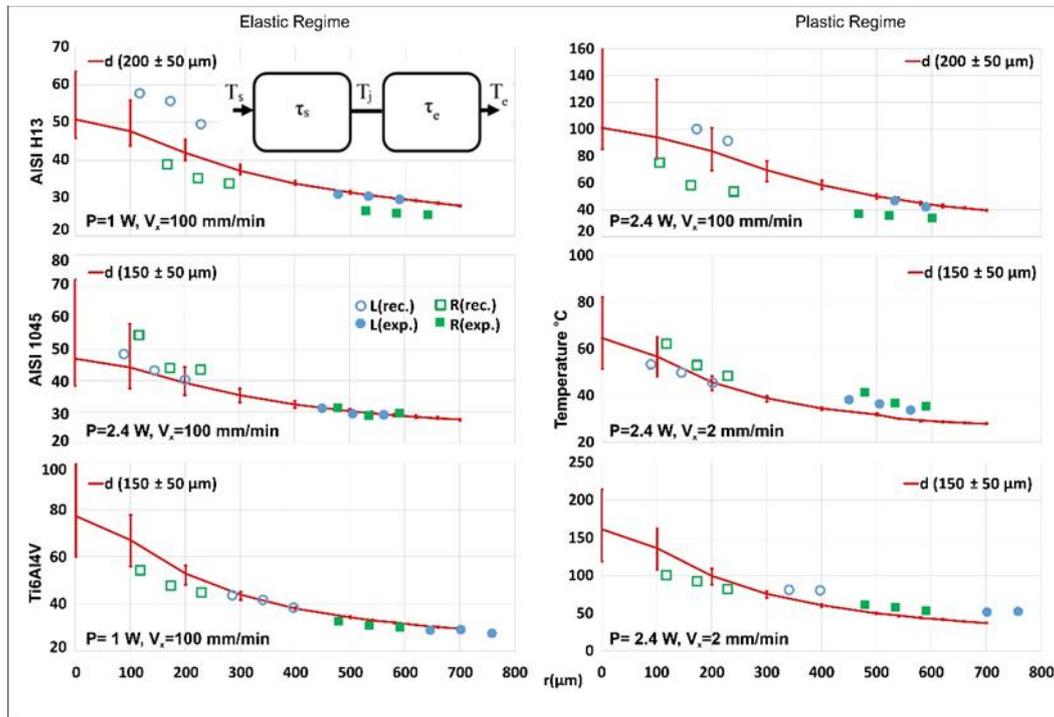

Figure 2.6 Experimental and FEM results of temperature in relation to distance from the laser beam centre, for the elastic (left column) and plastic (right column) regimes of the three materials [14]
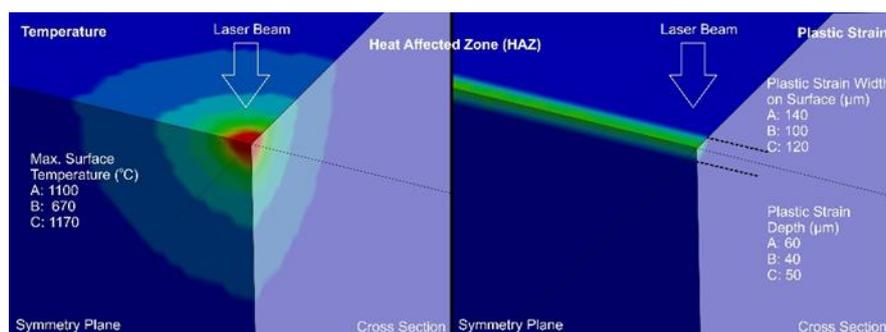

Figure 2.7 HAZ. Temperature distribution (left) and plastic strain width and depth (right)

A. Baroutsos
Tracking, analysis, and interference in FEM solution subdomains in simulations of laser assisted machining.

ippl

Chapter 3

3 Analyzing, Tracking, Selecting, Processing Sub-regions

In this chapter the steps of locating and extracting the maximum AOI sub-region results from LS-PREPOST are analyzed. The method of analyzing/filtering these data on Linux Operating System (OS) using GNU Bash or just Bash shell is described. The aim is to create a universal tool that should work on every Linux distribution, using only standard and universal script coding.

The processing of sub-regions of a FEM model simulating LAM, is essential to improve machinability by investigating phenomena such as the generation of built-up edge, the chip formation or the tool wear. In this chapter will be addressed the needed steps to analyze, track, select and process sub-regions of maximum interest. These sub-regions could be used as initial conditions for different types of simulations such as MHD plasma or molecular dynamics simulations.

3.1 Data processing

A characteristic LAMM model was selected to process the sub-regions of high interest. The sub-regions were selected having as criterion the quantity of temperature. A typical temperature distribution in the workpiece model is presented in figure 2.7.

3.1.1 Initial attempts

The first attempt to access data was made by converting directly the LS-DYNA output files to HDF5 format [20], but all attempts failed to produce a stable and universal tool that would work in every Linux distribution without the need to rewrite code, or without having difficulties to access, install and use all the needed libraries, especially on High-Performance Computers (HPC's).

The first attempts were performed with qd, which is a CAE (Computer Aided Engineering) Python library [21]. These libraries, when properly installed, can directly access

A. Baroutsos
Tracking, analysis, and interference in FEM solution subdomains in simulations of laser assisted machining.

ippl

LS-DYNA solver's outputs (d3plot or binout files) and convert them to HDF5 open-source format files. The most difficult task was the installation and proper usage of pybind library [22], which as creators mention in their online documentation *"pybind11 is a lightweight header-only library that exposes C++ types in Python and vice versa, mainly to create Python bindings of existing C++ code"*[2]. It is an important tool for the proper usage of C++ code in Python scripts. While in common Linux distributions it is easy to be installed, in professional and commercial distributions the installation difficulties increase. The installation on the HPC GR-NET ARIS[3], under the project ID pr005024-LaMIPlaS [13], was very complicated and time consuming. The next attempt was made by using D3PLOT2HDF5 commercial software from TAILSIT team[4]. It is a standalone executable, not dependent on the system software configuration that uses single line bash script and can only convert D3PLOT type of LS-DYNA outputs, derived from symmetric multiprocessing (SMP) type of solvers. However, we needed to use it in massively parallel processors (MPP) solvers, which require the usage of message passing interface (MPI) and provide only BINOUT type of outputs. Therefore, D3PLOT2HDF5 could not operate in computer clusters and especially in ARIS HPC, since in these installations only MPP or variations of MPP, like hybrid parallel computing, can be used. Simultaneously, attempts of using MATLAB / OCTAVE software to analyze final data were unsuccessful due to the vast amount of needed time to edit matrices of more than 100000 rows. This process has a duration of more than 4 hours, while the usage of stream editors needs a few minutes. These failed attempts were essential to guide us to develop a universal tracking and analysis code in Linux bash script.

3.1.2 Tracking and analysis of sub-regions in Linux bash

Using Linux bash shell for analyzing mathematical data is not a common method. Nevertheless, if it is successful, a universal tool can be created. First task to be done is to export simulation results from LS-PREPOST (figure 3.1) in a form that can be edited and handled easily using bash kernel stream editors. LS-PREPOST can export core data of each solution step as ASCII file. The data that can be exported in ASCII file for each solution step are:

1. *ELEMENT_SOLID*: id of each element and the nodes that belong to it.
2. *NODE*: id of each node and its x, y, z position.

---

[2] pybind11, url: https://pybind11.readthedocs.io/en/latest/intro.html, last accessed : 17 April 2020
[3] Webpage of ARIS HPC https://hpc.grnet.gr/ last accessed: 17 April 2020.
[4] Webpage and download site of D3PLOT2HDF5 https://www.tailsit.com/d3plot2hdf5.en.shtml#start, TailSiT GmbH. Free for not commercial use.

A. Baroutsos
Tracking, analysis, and interference in FEM solution subdomains in simulations of laser assisted machining.

ippl

3. *INITIAL_VELOCITY_NODE*: initial x, y, z speed for each node.

4. *NODAL_DISPLACEMENT*: the displacement for each node from their initial position in step 0.

5. *RESULT OF Temperature*: the temperature for each node.

6. *SOLID_ELEMENT_CENTROID*

   a. *Eid, X, Y, Z, Volume,* centroid x,y,z position and volume for each element

   b. *Total Solid element Volume,* the total workpiece volume
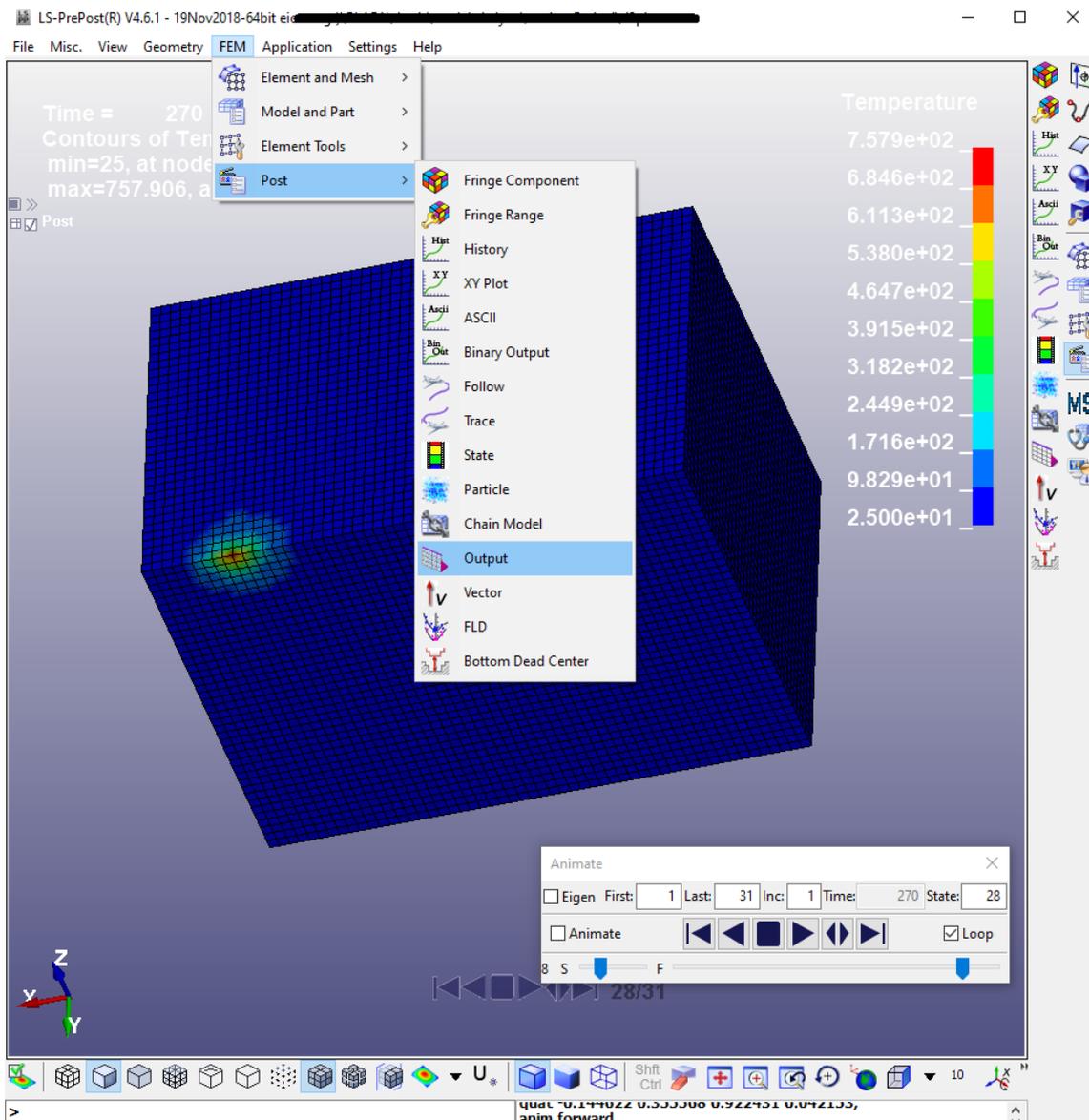

Figure 3.1 Solution set extraction as ASCII in LS-PREPOST

All, the above, are the minimum amount of data, that are extracted from the simulation solution since other physical quantities (such as von mises stresses and strains) are derived using proper mathematical expressions.

A. Baroutsos
Tracking, analysis, and interference in FEM solution subdomains in simulations of laser assisted machining.

ippl

Since there are solution data, in a format that can be filtered by bash kernel tools, the next step is to filter them, to track and obtain only the AOI. For LAMM tracking of the AOI the procedure is simple since it can be done by filtering the temperature data.

The first step is to filter the nodes that have temperature above a selected threshold. Then the elements, that the filtered nodes belong to, are selected. The final nodes list is created by assembling the nodes of these elements. Having these two types of data filtered, then using the ids of the elements and the nodes, the whole data set of the simulation solution outputs can be filtered and tracked and be further analyzed to determine the sub-regions of the maximum interest.

3.2 Analysis of sub-regions of maximum interest and comparison with the pre-filtered model

Filtering the solutions' outputs of the workpiece simulation models, results to an extreme smaller solution domain, neglecting less significant data. These data can be handled faster, providing us with all the important information for the model, since less computation time and small file sizes are handled. Three successive solution timestep files where used. The temperature threshold was selected to be the 10% of the maximum temperatures. The three
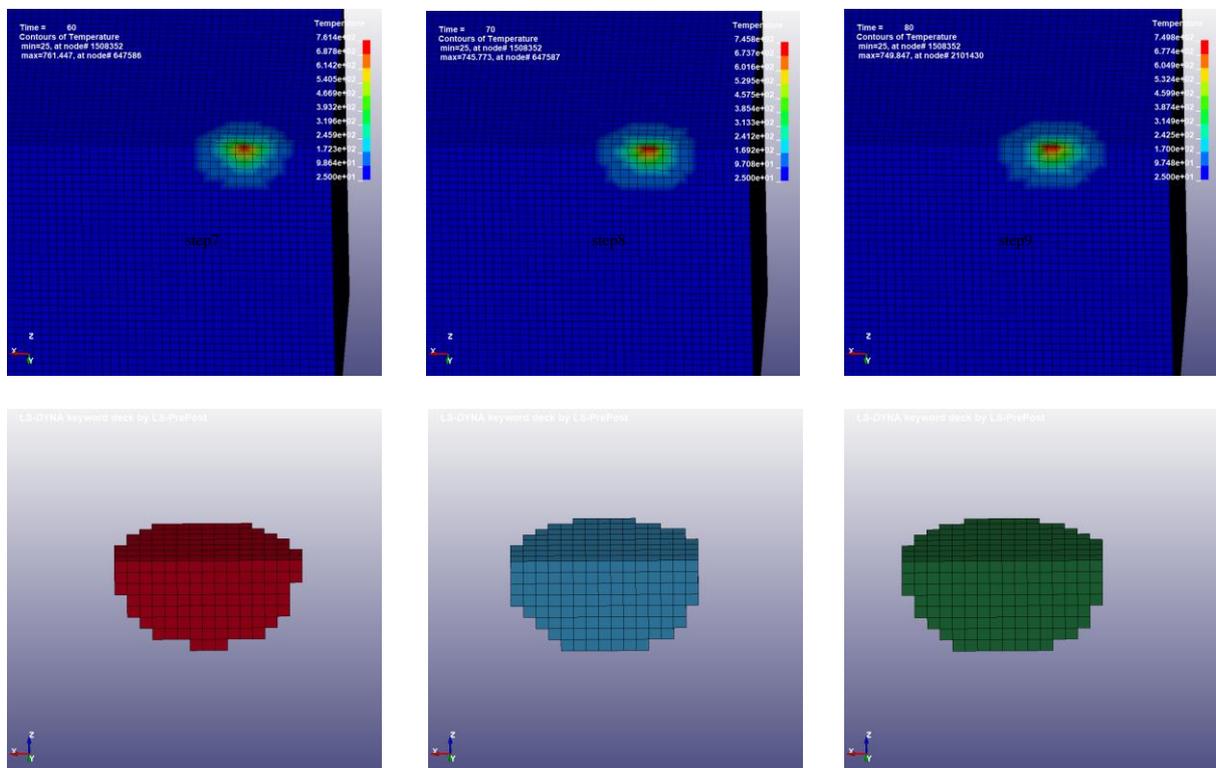

Figure 3.2 Three successive timesteps of the simulation's solution. Top figure shows solution before tracking the sub-region of maximum interest. Bottom figure shows the region of maximum interest after filtering.

21

A. Baroutsos
Tracking, analysis, and interference in FEM solution subdomains in simulations of laser assisted machining.

ippl

time-step solution files that resulted from the above filtering had a size of 198 kb, 233 kb and 250 kb, while prior to filtering each time-step solution file size was 25218 kb. A size reduction of ~100 times, to locate and track only the AOI is achieved. The following figures demonstrate the tracked sub-region of maximum interest.
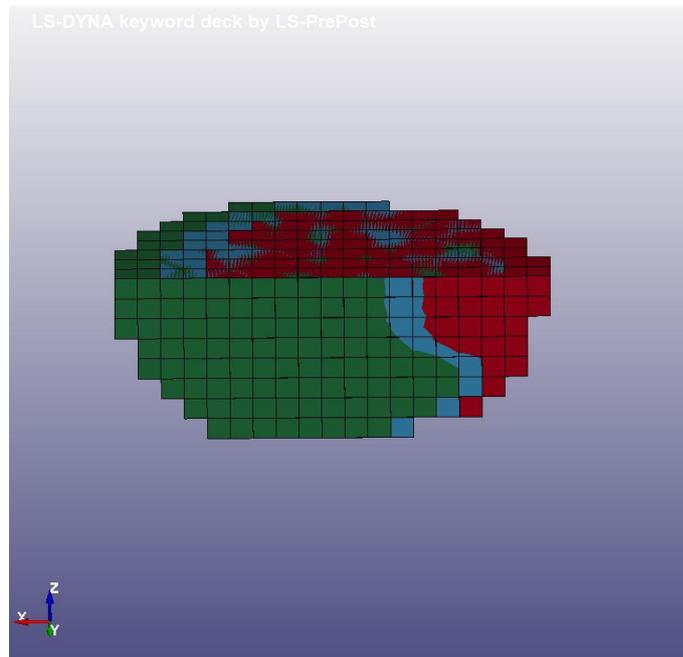

Figure 3.3 All three tracked sub-regions merged with different color, where offset between these three steps are obvious

It is clear in figures 3.2 and 3.3 that we selected the nodes and the elements of the AOI sub-region. This tracking is essential since these data can be further used as potential initial conditions for MHD plasma or molecular dynamics simulations.

3.3 Linux bash script code

The tracking and filtering of the AOI sub-regions code developed in the Linux bash script code is here explained:

The main code body is:

1. *#!/bin/bash*
2. *csplit -k -s -n 1 <output ls-prepost file> /*KEYWORD/ {*}*
3. *rm -f xx0*
4. *sed -n '/$RESULT OF Temperature/,/[$]/{x;p;}' <xx*>temperature**
5. *sed -i -e '1,2d' -e 's/.\{10\}/& /g' temperature**
6. *sort -r -k 2 -g -o temperature* temperature**
7. *THRESTEMP=$(awk 'BEGIN {print ('$(awk 'NR==1 -n {print $2}' temperature*)'* 0.1)}')*
8. *awk '{if ($2>='$THRESTEMP'){print $1} else exit 1}' <temperature* >elements*

22

A. Baroutsos
Tracking, analysis, and interference in FEM solution subdomains in simulations of laser assisted machining.

ippl

9. *sed -n '/*ELEMENT_SOLID/,/[*]/{x;p;}' <xx* >elements**

10. *sed -i '1,2d' elements**

11. *./script1 >finalelements*

12. *./script2 >onecolumn*

13. *sort -g -u -o onecolumn onecolumn*

14. *sed -n '/*NODE/,/[*]/{x;p;}' <xx* >node**

15. *sed -i '1,2d' node**

16. *./script3 >finalnodes*

17. *awk '{print $1}' <finalelements >onecolumnelements*

18. *head -5 xx* >final**

19. *cat finalelements >>final**

20. *echo *NODE >>final**

21. *cat finalnodes >>final**

22. *sed -n '/*INITIAL_VELOCITY_NODE/,/[*]/{x;p;}' <xx* >initialvelo**

23. *sed -i -e '1,2d' -e 's/.\{10\}/& /g' initialvelo**

24. *./script4 >testinivel*

25. *awk '{print substr ($0,1,10) substr($0,12,10) substr($0,23,10) substr($0,34,10)}' testinivel >testinivelcorrect*

26. *echo *INITIAL_VELOCITY_NODE >>final**

27. *cat testinivelcorrect >> final**

28. *echo *END >> final**

29. *sed -n '/$NODAL_DISPLACEMENT/,/[$]/{x;p;}' <xx* >noddispl**

30. *sed -i '1,2d' noddispl**

31. *./script5 >testnoddispl**

32. *echo $NODAL_DISPLACEMENT >>final**

33. *cat testnoddispl* >> final**

34. *echo $NODAL_RESULTS >> final**

35. *sed -n '/$RESULT OF Temperature/,/[$]/{x;p;}' <xx* >temperature**

36. *sed -i -e '1,2d' -e 's/.\{10\}/& /g' temperature**

37. *./script6 >testtemperature**

38. *awk '{print substr ($0,1,10) substr($0,12,10)}' testtemperature* > testtemperaturecorrect*

39. *echo $RESULT OF Temperature >> final**

40. *cat testtemperaturecorrect >> final**

41. *echo $SOLID_ELEMENT_CENTROID*

42. *sed -n '/$Eid, X, Y, Z, Volume/,/[$]/{x;p;}' <xx* > elemvol**

43. *sed -i '1,2d' elemvol**

44. *./script7 >testelemvol**

45. *echo $Eid, X, Y, Z, Volume >> final**

46. *cat testelemvol* >> final**

47. *sed -n -e '$p' xx* >> final**

23

A. Baroutsos
Tracking, analysis, and interference in FEM solution subdomains in simulations of laser assisted machining.

ippl

The seven sub-scripts:

- script 1:

```
#!/bin/bash
filename='elemets'
while read line; do
cat elements* | grep -w $line | awk '{if (($3=='$line') || ($4=='$line') || ($5=='$line') || ($6=='$line') || ($7=='$line') || ($8=='$line') || ($9=='$line') || ($10=='$line'))  print $0 }'
done <$filename
```

- script 2:

```
#!/bin/bash
for i in {3..10}
do
  cat finalelements | awk '{print $'$i'}'
done
```

- script 3:

```
#!/bin/bash
filename='onecolumn1'
while read line; do
cat node* |grep -w $line | awk '{if (($1=='$line')) print $0}'
done <$filename
```

- script 4:

```
#!/bin/bash
filename='onecolumn1'
while read line; do
cat initialvelo* |grep -w $line | awk '{if (($1=='$line')) print $0}'
done <$filename
```

- script 5:

```
#!/bin/bash
filename='onecolumn1'
while read line; do
cat noddispl* |grep -w $line | awk '{if (($1=='$line')) print $0}'
done <$filename
```

- script 6:

```
#!/bin/bash
filename='onecolumn1'
while read line; do
cat temperature* |grep -w $line | awk '{if (($1=='$line')) print $0}'
done <$filename
```

A. Baroutsos
Tracking, analysis, and interference in FEM solution subdomains in simulations of laser assisted machining.

ippl

- script 7:

```
#!/bin/bash
filename='onecolumnelements'
while read line; do
cat elemvol* |grep -w $line | awk '{if (($1=='$line')) print $0}'
done <$filename
```

where <filename>* means the specific filename for a certain step (xx8)

In line 2 of the main code simulation's results file is split in separate solutions files for every simulation step and in line 3 the empty file xx0 is deleted. In lines 4-6 temperature data from xx* step solution file, are selected, formatted and sorted, in line 8. The THRESTEMP variable selects the nodes which are above the given threshold, which in our case is the 10% of the maximum temperature. Line 9 works like line 4 for the elements and line 10 deletes the first 2 lines. Script 1, in line 11, selects the elements that has nodes with temperature over the threshold. Script 2, in line 12, selects all nodes from the previous script and place them in one column, while in line 13 they are sorted, and all duplicate lines are removed. This is done to select the proper part of the node data. In line 14 we select all the node data, in line 15 the first 2 rows are deleted, and in line 16, script3 outputs the final nodes filtered data. Next in line17 we create the list of the filtered elements. First 5 rows of solution are copied in line 18 and the filtered elements are copied in line 19. After the elements and nodes must be copied. In line 20 the node's flag and in line 21 the selected nodes are copied. Initial velocity is derived from the solution, which is formatted in lines 22 and 23 respectively, then it is filtered by script 4 and in lines 25, 26 and 27 is reformatted, while the flag and the selected initial nodal speeds are copied to the new filtered solution. In line 28 we copy the *END flag. After initial velocity, nodal displacement, temperature, and centroid element data are similarly selected and copied to the new AOI solution.

3.4 Restart code for interference with the solution

Restarting the solution of a simulation, allows to correct or modify parameters of the problem at any step of the solution. This is a procedure, that may be impossible or not feasible, during an actual experiment. The code, that is created in paragraph 3.3 allow us to quickly locate and analyze the sub-regions of interest, and then a restart code is developed to modify the key parameters and restart the solution of the problem, at the proper time step.

A. Baroutsos
Tracking, analysis, and interference in FEM solution subdomains in simulations of laser assisted machining.

ippl

To make restart feasible and automatic, two Linux bash scripts are developed. The first removes the initial temperature node values and replaces them with new recalculated initial temperature values. The second one alters the name of the main function's name and can be further edited to make changes in mathematical functions. These scripts can be further combined with the output of other simulation solvers, such as molecular dynamics or HD/MHD problems:

- script *MakeFullrestart*

```
#!/bin/bash
read -p 'File name of .k we want to make restart file : '
sed -i.bak '/*INITIAL_TEMPERATURE_SET/,/["*"]/{x;d;}' ${REPLY}
mv ${REPLY} testfullre.k
mv $(printf ${REPLY}.bak) ${REPLY}
sed -i '/*INITIAL_TEMPERATURE_NODE/,/["*"]/{x;d;}' testfullre.k
sed -i '/*END/i *INITIAL_TEMPERATURE_NODE' testfullre.k
read -p 'File name which contains the nodal temperature values : '
TEST3=${REPLY}
echo $TEST3
sed -i -e "/*INITIAL_TEMPERATURE_NODE/r $TEST3" testfullre.k
```

- script ChangeFunction

```
#!/bin/bash
read -p 'File name of fullrestart file: '
TEST="$(grep g[0-9][0-9] ${REPLY})"
TEST1=${TEST:1:2}
TEST1="$(expr $TEST1 + 1)"
TEST1="$(printf "%02d\n" $TEST1)"
TEST2=${TEST:0:3}
TEST3="$(printf ${TEST:0:1}$TEST1)"
sed -i "s/$TEST2/$TEST3/g" ${REPLY}
```

The script MakeFullrestart, creates a new keyword file, where the initial temperature values are removed to avoid confliction with the temperature values that the nodes obtain during the solution procedure. The new keyword file is called testfullre.k. The second script ChangeFunction, simply renames the function of the new keyword file, by adding +1 to the

A. Baroutsos
Tracking, analysis, and interference in FEM solution subdomains in simulations of laser assisted machining.

ippl

special formatted name (<name>[number][number]). The new restart file continues the solution from the point of the interruption.

3.5 Simulation results using the restart code and interference with the simulation parameters

In figures 3.4-3.29 are depicted simulation results of temperature distribution, plastic strain, Von Mises stress and the cutting x-force and the thrust y-force. For the reference-REF model where, no restart is considered. The cutting and laser speed is 2.5 m/sec and the laser heat flux is 0.16 kW/mm^2. Cutting is initiated 0.25 ms after the initiation of laser scanning. The restart code is used in two different models. In the first restart model-RES1, when restart analysis starts, the laser heat flux increases from 0.16 kW/mm^2 to 2.5 kW/mm^2, while for the second restart model-RES2, when restart analysis is initiated, the cutting speed increases from 2.5 m/sec to 5 m/sec. For both models the restart analysis is initiated at 0.29 ms. A feed rate values of 0.15 mm/rev is considered for all three models.

In figures 3.4 to 3.9 are depicted simulation results of the temperature distribution of LAM for the AISI H-13 steel workpiece for the REF, RES1, RES2 models and for two different temporal moments.
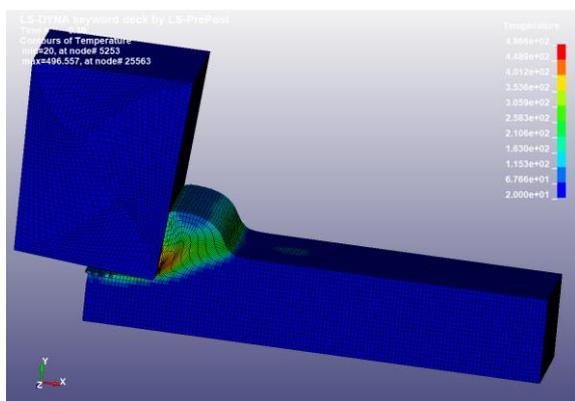
Figure 3.4 Temperature distribution at time 0.39 ms, for the REF model
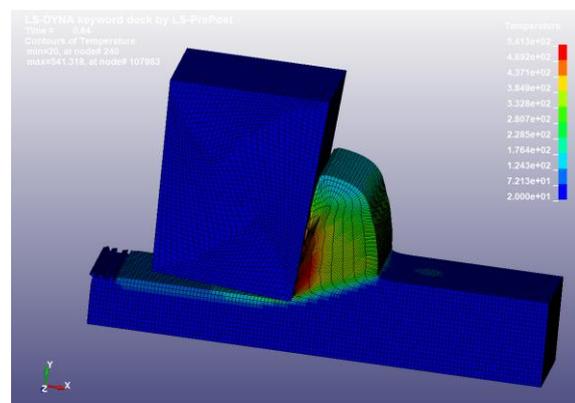
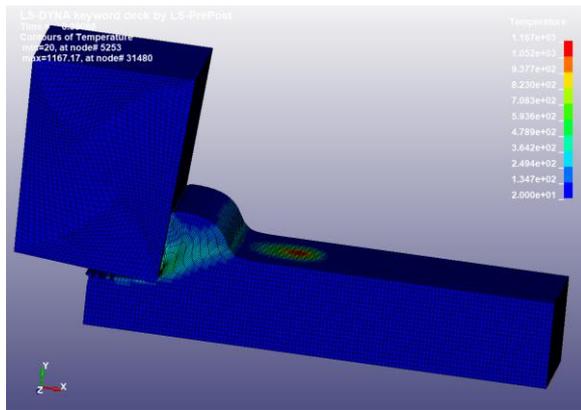**Figure 3.5** Temperature distribution at time 0.64 ms, for the REF model

A. Baroutsos
Tracking, analysis, and interference in FEM solution subdomains in simulations of laser assisted machining.

ippl

Figure 3.6 Temperature distribution at time 0.39 ms, for the RES1 model
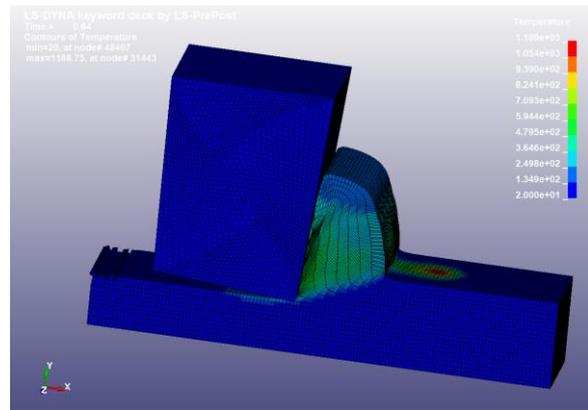

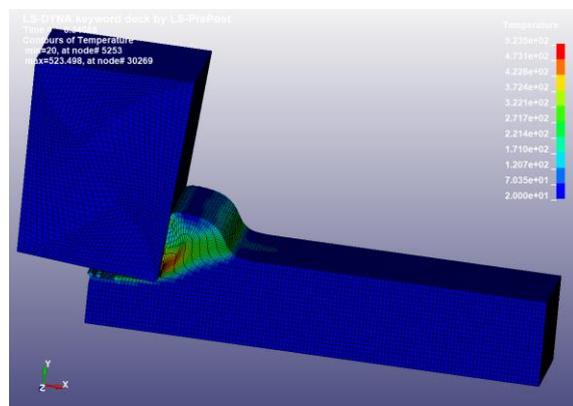**Figure 3.7** Temperature distribution at time 0.64 ms, for the RES1 model

Figure 3.8 Temperature distribution at time 0.34 ms, for the RES2 model. The cutting tool has moved the same distance as in the REF model at 0.39 ms
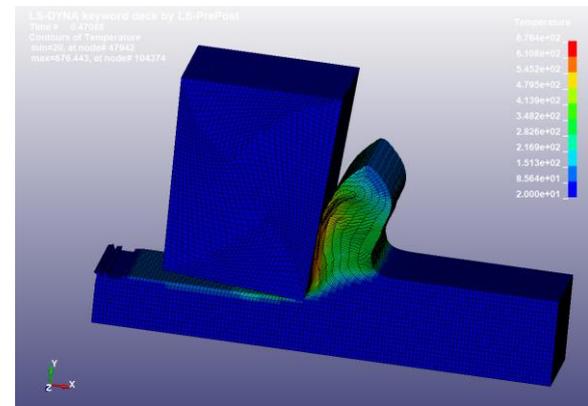

Figure 3.9 Temperature distribution at time 0.47 ms, for the RES2 model. The cutting tool has moved the same distance as in the REF model at 0.64 ms

In the REF model an 8% maximum temperature increase is observed between the two temporal moments of 0.39 ms and 0.64 ms (figures. 3.4, 3.5). This is attributed to the evolution of the cutting process. The difference of the maximum temperatures between the REF and the RES1 models are about 600 to 650 °C, for both temporal moments, as can be seen in figures 3.4-3.7. On the contrary in the RES1 model, for both temporal moments the temperature remains stable (~1168 °C), which is below the AISI H-13 steel melting point (1427 °C) and is suitable for the reduction of forces that occurs in LAM machining. Comparing the REF and the RES2 models there is increase of temperature in the RES2 model due to the increase of speed during cutting. For the same cutting distance of the tool, an increase of 5.4% is observed for the maximum temperature in figure 3.8 (RES2 model) when compared to the corresponding one in figure 3.4 (REF model). Likewise, comparing the maximum temperatures for the second temporal moments (0.47 ms–0.64 ms) in figures 3.5 and 3.8. an increase of 20% is observed

28

A. Baroutsos
Tracking, analysis, and interference in FEM solution subdomains in simulations of laser assisted machining.

ippl

for the maximum temperature in figure 3.9 (RES2 model). For the RES2 comparing the maximum temperature for figures 3.8 and 3.9 at 0.34 ms and 0.64 ms respectively, an increase of 23 % is observed, showing that when the cutting speed is higher the heating of the workpiece increases compared to the slower cutting speed.
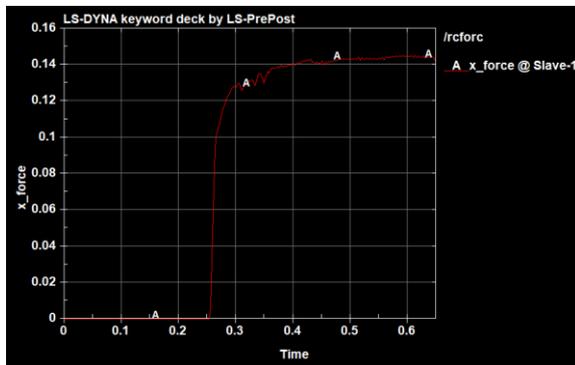

Figure 3.10 Cutting force in relation to time for the REF model. The maximum value of 0.16 for the cutting force corresponds to 320 N/mm, while time is in ms
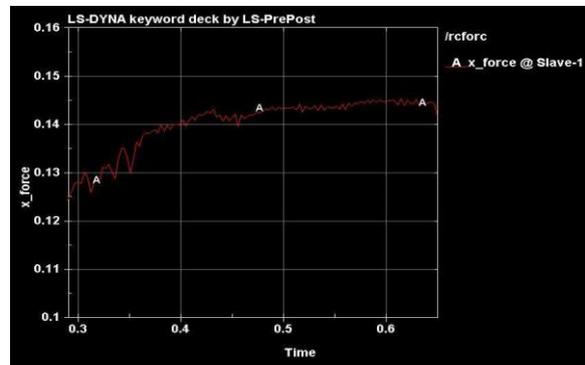
Figure 3.11 Cutting force in relation to time for the REF model starting from restart time 0.29 ms
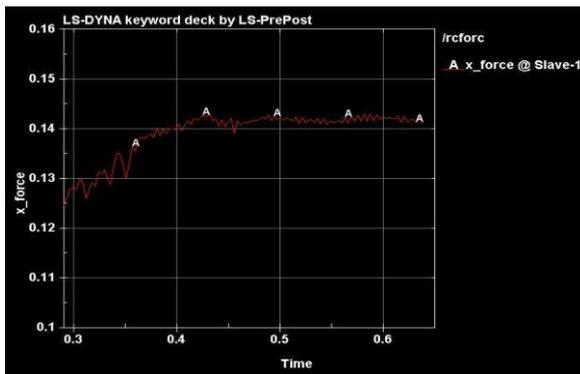
Figure 3.12 Cutting force in relation to time for the RES1 model starting from restart time 0.29 ms
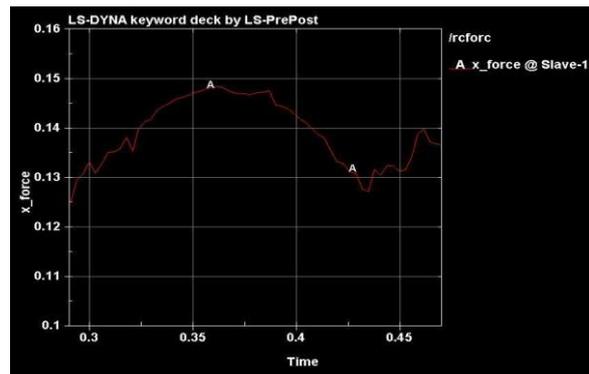

Figure 3.13 Cutting force in relation to time for the RES2 model starting from restart time 0.29 ms

In figures 3.10-3.13 are presented diagrams of the cutting force in relation to time for the three REF, RES1 and RES2 models. In figure 3.10 is presented the cutting force in relation to time for the REF model, while in figure 3.11 is the same model for initial restart time 0.29 ms. In figures 3.10 and 3.11 is presented the cutting force in relation to time for the RES1 and RES2 models, respectively. The movement of the cutting tool is initiated at 0.25 ms, as can be seen in figure 3.10, while the laser beam irradiation starts at the initial time of the simulation. In figures 3.11–3.13 the same range of values is used for better comparison after restarting the problem. Comparing cutting force results for the REF and RES1 models (figures 3.11, 3.12) after 0.45 ms the RES1 the mean cutting force is ~2.5 % lower than the respective of the REF model, while before 0.45 ms a low difference of ~0.1% is observed. This proves that the effects of the heat flux increase demand time to reduce the cutting force that acts on the workpiece.

A. Baroutsos
Tracking, analysis, and interference in FEM solution subdomains in simulations of laser assisted machining.

ippl

When comparing the cutting force results of the RES2 model with the REF model it is observed that the mean force increases with the speed increase. This percentage of increase is about 4.5% between 0.29-0.47 ms. The behavior of the cutting force is also different compared to the REF and RES1 models, since higher variations of the force are observed between 0.29-0.47 ms. This behavior is attributed to the increase of speed, therefore more time is needed for the cutting force to be stabilized with variations. The heating of the workpiece due to the higher cutting speed decreases its hardness.
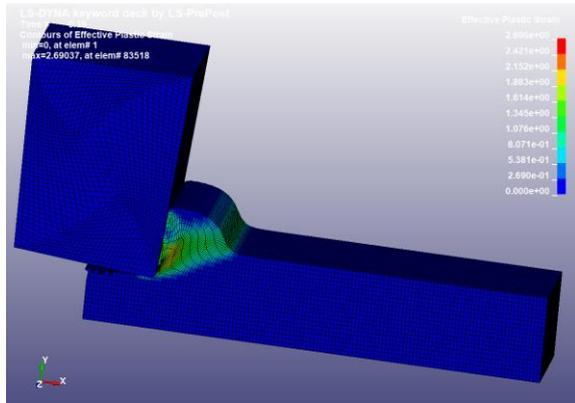
Figure 3.14 Plastic strain distribution at time 0.39 ms, for the REF model
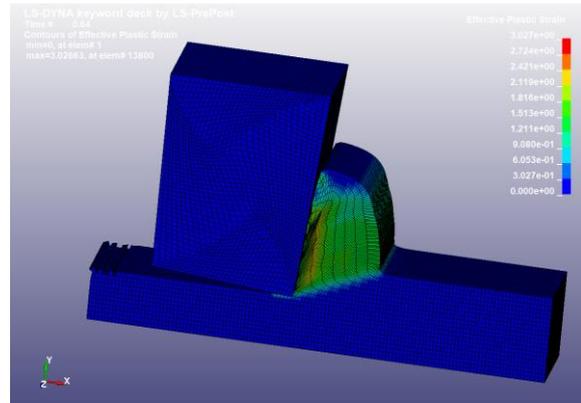

Figure 3.15 Plastic strain distribution at time 0.64 ms, for the REF model
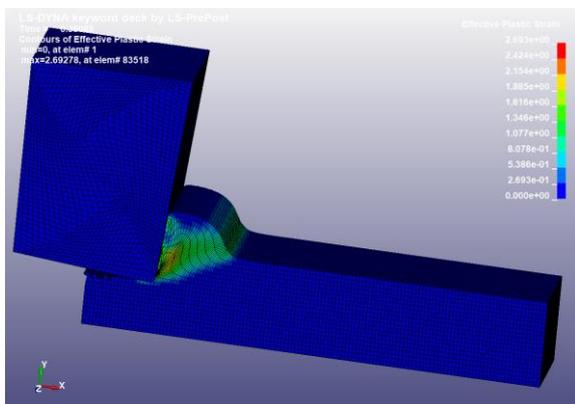

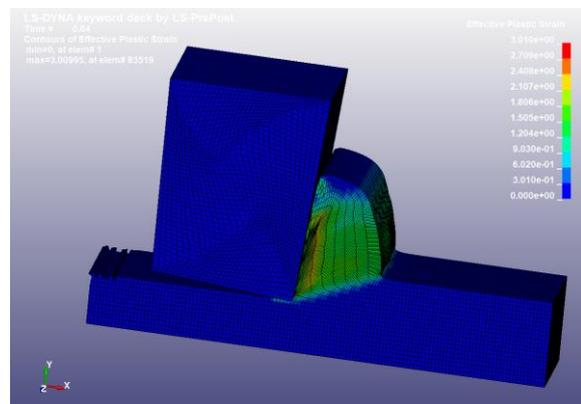**Figure 3.16** Plastic strain distribution at time 0.39 ms, for the RES1 model

Figure 3.17 Plastic strain distribution at time 0.64 ms, for the RES1 model

A. Baroutsos
Tracking, analysis, and interference in FEM solution subdomains in simulations of laser assisted machining.
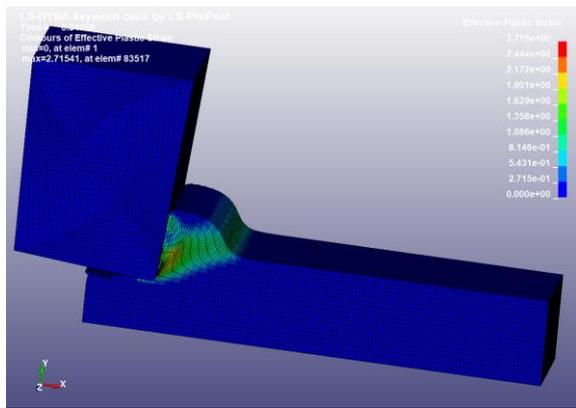
ippl

Figure 3.18 Plastic strain distribution at time 0.34 ms, for the RES2 model. The cutting tool has moved the same distance as in the REF model at 0.39 ms
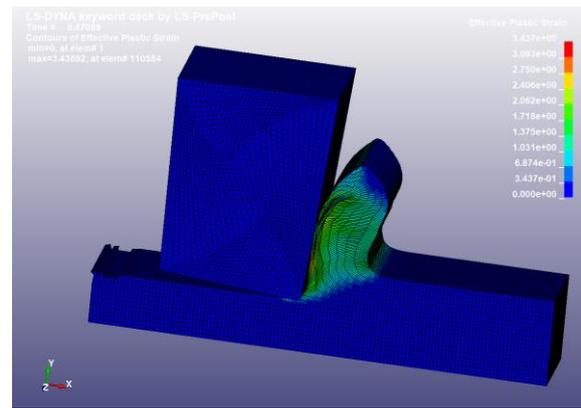
Figure 3.19 Plastic strain distribution at time 0.47 ms, for the RES2 model. The cutting tool has moved the same distance as in the REF model at 0.64 ms

Plastic strain is a physical quantity that demonstrates the permanent deformations of the workpiece due to the machining process. The REF and RES1 models present negligible differences regarding the developed plastic strain distribution (figures 3.14 -3.17). This occurs since the developed strains due to cutting are much higher than the developed strains due to laser heating, therefore the increase of the temperature distribution in the RES1 model, due to higher laser fluence, does not influence the developed plastic strains. The first temporal instant (times 0.39 ms and 0.34 ms for figures 3.14 and 3.18 respectively) the RES2 model develops about 1% higher maximum plastic strain compared to the REF model. However, for the second temporal instant this percentage increases to ~11.9% (times 0.64 ms and 0.47 ms for figures 3.15, and 3.19 respectively). This occurs since the cutting speed is doubled for the RES2 model and the impact is higher. Comparing figure 3.15 to figure 3.19 a different chip formation is observed due to the increased value of speed.
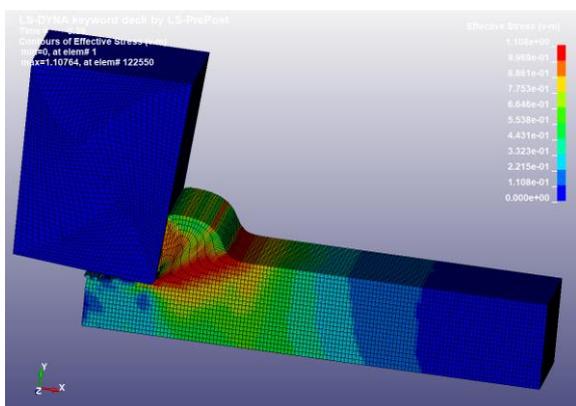

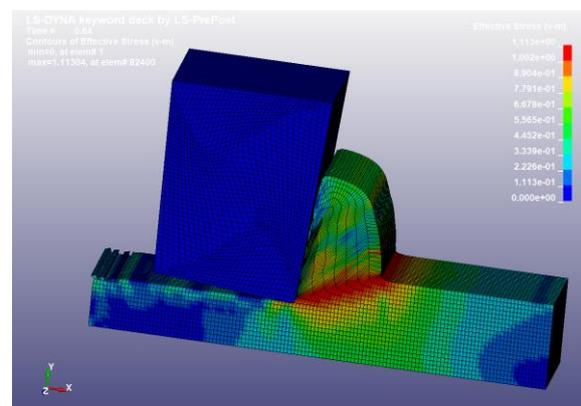**Figure 3.20** V-M stress distribution (in GPa) at time 0.39 ms, for the REF model

Figure 3.21 V-M stress distribution at time 0.64 ms, for the REF model

31

A. Baroutsos
Tracking, analysis, and interference in FEM solution subdomains in simulations of laser assisted machining.
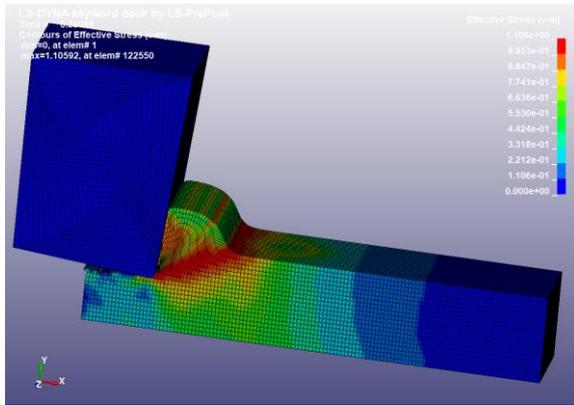
ippl

Figure 3.22 V-M stress distribution at time 0.39 ms, for the RES1 model
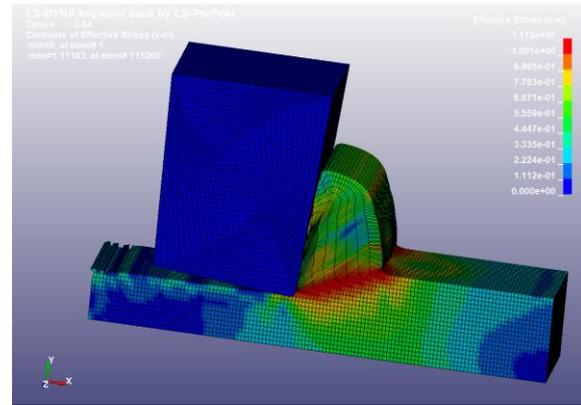

Figure 3.23 V-M stress distribution at time 0.64 ms, for the RES1 model

Figure 3.24 V-M stress distribution at time 0.34 ms, for the RES2 model. The cutting tool has moved the same distance as in the REF model at 0.39 ms

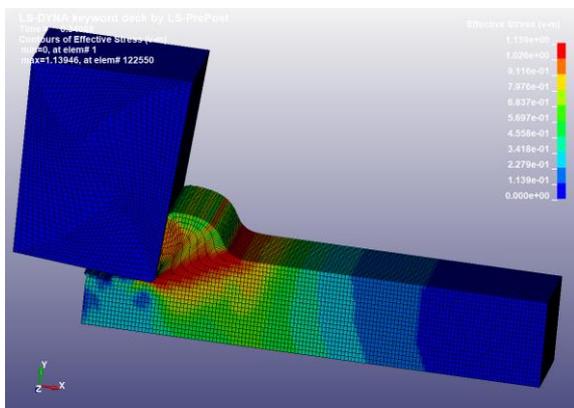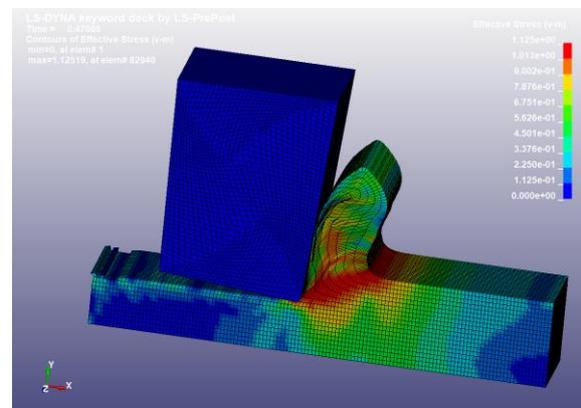
Figure 3.25 V-M stress distribution at time 0.47 ms, for the RES2 model. The cutting tool has moved the same distance as in the REF model at 0.64 ms

The developed Von Mises (V-M) stresses on the workpiece are depicted in figures 3.20 to 3.25. For all three models the V-M stress distribution is following a similar behavior. The difference of the maximum V-M stress between the REF model and the RES1 model is less than 0.1%. This information are important for future experimental measurements to provide more efficient use of laser radiation. The RES2 model has a tendency to decrease the maximum V-M stress over time compared to the other 2 models and the maximum V-M stress of the RES2 model is about 2.8% and 1.1% higher than the REF and the RES1 model for the first and second temporal moments respectively.
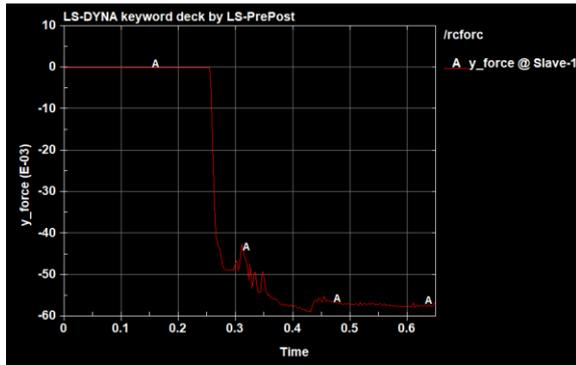
A. Baroutsos
Tracking, analysis, and interference in FEM solution subdomains in simulations of laser assisted machining.

ippl

Figure 3.26 Thrust force in relation to time for the REF model.
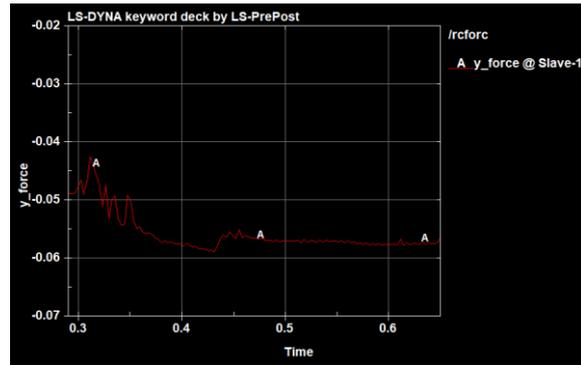

Figure 3.27 Thrust force in relation to time for the REF model starting from restart time 0.3 ms
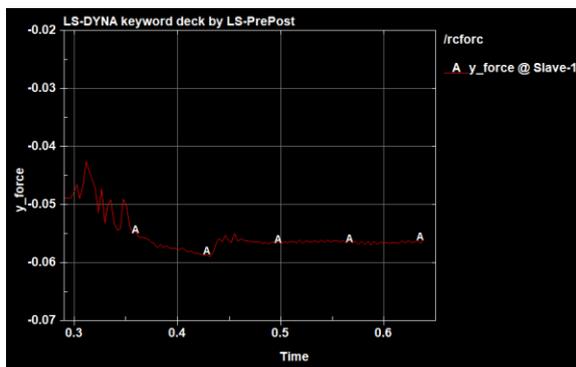

Figure 3.28 Thrust force in relation to time for the RES1 model starting from restart time 0.3 ms
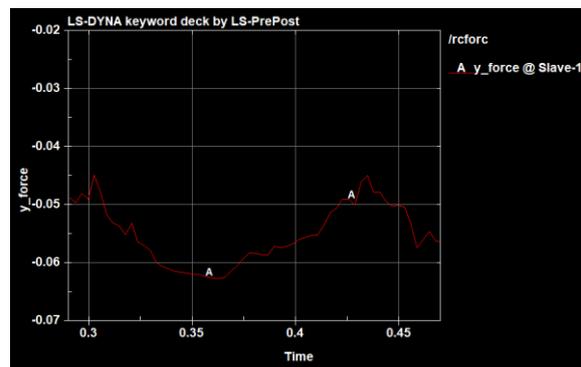
Figure 3.29 Thrust force in relation to time for the RES2 model starting from restart time 0.3 ms.

In figures 3.26-3.29 are presented diagrams of the thrust force in relation to time, following the same philosophy with the cutting forces. In figure 3.26 is presented the thrust force in relation to time for the REF model, while in figure 3.27 is the same model for initial restart time 0.29 ms. In figures 3.28 and 3.29 is presented the thrust force in relation to time for the RES1 and RES2 models, respectively. Comparing thrust force results for the REF and RES1 models (figures 3.27, 3.28) after 0.45 ms the RES1 mean cutting force is ~0.5% lower than the respective of the REF model. The behavior of the thrust force for the RES2 model is also different compared to the REF and RES1 models, since higher variations of the force are observed between 0.29-0.47 ms. Generally, it can be concluded that the thrust force follows the behavior of the cutting fore.

A. Baroutsos
Tracking, analysis, and interference in FEM solution subdomains in simulations of laser assisted machining.

ippl

Chapter 4

4 Conclusions

A universal tool that works for every Linux distribution, using only standard and universal script coding, was developed in this thesis, and was applied in the FEM simulation of LAM. LAM is a hybrid method that combines conventional machining and Laser light, in order to enhance cutting tool material removal. The main feature of the LAM process is the reduction of the cutting forces via increasing the temperature of the workpiece in order to reduce the strength of the material. This strength reduction causes the reduction of the material hardness and the tool's wear. Thus, the machinability of the workpiece is increased, the tool life is extended, and surface finish is improved, while high material removal rate is achieved. To further explore the LAM method and to reduce the performance cost of a large majority of experiments, computer simulation is a valuable tool for this complex hybrid method of machining.

The developed code is capable to analyze, track, select and process sub-regions of maximum interest during LAM FEM simulation and to restart FEM analysis when it is needed for interference. These sub-regions can be used as initial conditions for different types of simulations such as MHD plasma or molecular dynamics simulations and therefore to interconnect different numerical methods such as FEM-MHD, FEM-MD. These developed bash scripts are universal and can be the basis for further development till potentially a more automated or more dedicated software is developed to combine different numerical approaches.

A. Baroutsos
Tracking, analysis, and interference in FEM solution subdomains in simulations of laser assisted machining.

ippl

5 Bibliography

[1]   S. Kalpakjian and S. R. Schmid, Manufacturing Engineering an Technology 6th edition, Singapore: Pearsons Education South Asia, 2010.

[2]   W. Habrat, K. Krupa, A. P. Markopoulos and et al., "Thermo-mechanical aspects of cutting forces and tool wear in the laser-assisted turning of Ti-6Al-4V titanium alloy using AlTiN coated cutting tools.," *Int J Adv Manuf Technol,* 2020.

[3]   Π. Κ. Γκότσης, Πεπερασμένα Στοιχεία, Αθήνα: ΖΗΤΗ, 2005.

[4]   K. H. Huebner, D. L. Dewhirst, T. G. Byrom and D. E. Smith, The Finite Element Method for Engineers, 4th Edition, New York: Wiley-Interscience Publication, 2001.

[5]   R. Courant, "Variational methods for the solution of problems of equilibrium and vibrations," *Bulletin of the American Mathematical Society,* no. 49, pp. 1-24.

[6]   A. Hrennikoff, "Solution of problems of Elasticity by the Frame-Work Method," *ASME J. Appl. Mech,* no. 8, pp. A619-A715, 1941.

[7]   A. Baroutsos, *Bachelor Thesis"Building and optimizing of clusters in hardware and software in Linux OS for the parallel processing of numerical problems of high computer power demanding simulations.",* Chania: TEI of Crete, School of Applied Sciences, Department of Enviromental and Natural Resources Engineering., 2017.

[8]   J. H. Argyris, "Energy theorems and structural analysis," *Aircr.Eng.,* no. 26;27, pp. 341-356,383-387.394;42-58,80-94,125-134,145-158, 1954;1955.

[9]   M. J. Turner, R. W. Clough, H. C. Martin and L. C. Topp, "Stiffness and deflection analysis of complex structures," *J. Aeronaut. Sci.,* no. 23, pp. 805-823, 854, 1956.

[10]   J. H. Argyris, Energy Theorems and Structural Analysis, London: Butterworth, 1960.

[11]   O. C. Zienkiewicz and R. L. Taylor, The Finite Element Method, Vols. I-III, McGraw-Hill, 1967.

[12]   O. C. Zienkiewicz and R. L. Taylor, The Finite Element Method, Fifth ed., vol. I, Butterworth-Heinemann, 2000.

[13]   E. Kaselouris, A. Baroutsos, T. Papadoulis, N. A. Papadogiannis, M. Tatarakis and B. Dimitriou, "A Study on the Influence of Laser Parameters on Laser-Assisted Machining of AISI H-13 Steel," *Key Engineering Materials,* vol. 827, pp. 92-97, 2020.

[14]   E. Kaselouris, A. Skoulakis, Y. Orphanos, K. Kosma, T. Papadoulis, I. Fitilis , E. Clark, A. P. Markopoulos, M. Bakarezos, N. A. Papadogiannis, M. Tatarakis and V. Dimitriou, "Analysis of the Heat Affected Zone and Surface Roughness during Laser Micromachining of Metals," *Key Engineering Materials,* vol. 827, pp. 122-127, 2019.

A. Baroutsos
Tracking, analysis, and interference in FEM solution subdomains in simulations of laser assisted machining.

ippl

[15] J. O. Hallquist, LS-DYNA Theory Manual, California: Livermor Software Technology Corporation, 2006.

[16] G. Johnson and W. Cook, "A constitutive model and data for metals subjected to large strains, high strain rates and high temperatures," in *Proceedings of the 7th International Symposium on Ballistics*, 1983.

[17] G. Johnson and W. Cook, "Fracture Characteristics of Three Metals Subjected to Various Strains, Strain rates, Temperatures and Pressures,," *Engineering Fracture Mechanics,* vol. 21, no. 1, p. 31–48, 1985.

[18] R. Singh, M. J. Alberts and S. N. Melkote, "Characterization and prediction of the heat-affected zone in a laser-assisted mechanical micromachining process," *International Journal of Machine Tools & Manufacture,* vol. 48, p. 994–1004, 2008.

[19] E. Kaselouris , T. Papadoulis, E. Variantza, A. Baroutsos and V. Dimitriou, "A Study of Explicit Numerical Simulations in Orthogonal Metal Cutting," *Solid State Phenomena,* no. 261, pp. 339-346, 21 08 2017.

[20] T. H. Group, "Hierarchical Data Format, version 5," 1997-NNNN. [Online]. Available: https://www.hdfgroup.org/HDF5/.

[21] "QD-ENG ADVANCING CAE," [Online]. Available: http://www.qd-eng.de/. [Accessed 17 04 2020].

[22] "pybind11," [Online]. Available: https://pybind11.readthedocs.io/en/latest/intro.html. [Accessed 17 04 2020].

[23] J. P. Gordon, H. J. Zeiger and C. H. Townes, "The Maser---New Type of Microwave Amplifier, Frequency Standard, and Spectrometer," *Phys. Rev.,* vol. 99, no. 4, pp. 1264-1274, Aug 1955.

[24] A. L. Schawlow and C. H. Townes, "Infrared and Optical Masers," *Phys. Rev.,* vol. 112, no. 6, pp. 1940-1949, 1958.

[25] M. Jazman, "https://www.slideshare.net/," [Online]. Available: https://www.slideshare.net/deactivatepy/pohl-van-genderen-2017p5-figure-12-electromagnetic-spectrum-with-wavelengths-and-frequencies-used. [Accessed 29 1 2020].

[26] wikipedia.org. [Online]. Available: https://en.wikipedia.org/wiki/Stimulated_emission#/media/File:Stimulated_Emission.svg. [Accessed 29 1 2020].

[27] K. Venkatesan, R. Ramanujan and P. Kuppan, "Laser Assisted Machining of difficult to cut materials: Research Opportunities and Future Directions - A comprehensive review," in *Procedia Engineering 97 (2014)*, 12th GLOBAL CONGRESS ON MANUFACTURING AND MANAGEMENT, GCMM 2014.

A. Baroutsos
Tracking, analysis, and interference in FEM solution subdomains in simulations of laser assisted machining.

ippl

[28] G. Chryssolouris, N. Anifantis and S. Karagiannis, "Laser Assisted Machining: An Overview," *Transactions of the ASME,* vol. 119, pp. 766-769, 1997.

[29] E. Kaselouris, T. Papadoulis, A. Skoulakis, A. Baroutsos, I. Fitilis, Y. Orphanos, E. Bakarezos, N. A. Papadogiannis, M. Tatarakis and B. Dimitriou, "SIMULATIONS OF LASER ASSISTED MACHINING AND CONVENTIONAL CUTTING OF AISI H-13 STEEL," in *9th GRACM International Congress on Computational Mechanics*, Chania, 2018.